1.6

Meteorological Model Simulations in Support of Developing a Visibility Improvement Strategy for the Southeast US

Donald T. Olerud, Jr., Aaron P. Sims, John N. McHenry, and Robert E. Imhoff
Baron Advanced Meteorological Systems, Research Triangle Park, NC

1. INTRODUCTION

In recent years visibility concerns have come to the forefront in the air quality community. Millions of visitors to national parks in the United States have their views obstructed by pollution-induced haze. The USEPA reports that average visibility in the east has been reduced from 90 miles to 15-25 miles (http://www.epa.gov/oar/visibility/what.html). To address this issue, the USEPA in 1999 instituted policies to improve visibility in the national parks. As part of this initiative, five multi-state regional planning organizations (RPO) were formed. The RPO governing visibility issues in the southeastern US is the Visibility Improvement State and Tribal Association of the Southeast (VISTAS) (http://www.vistas-sesarm.org/).

VISTAS recognizes the regional nature of haze, and has therefore set up a modeling approach to address the problem in the southeast US. Ultimately pollution controls will be enacted based upon chemical modeling results over the region of interest. To support this modeling effort, Baron Advanced Meteorological Systems (BAMS) is tasked with conducting the meteorological modeling. A 12-month modeling period is deemed necessary to cover an adequate range of visibility impairment. Prior to investing the resources to produce meteorological results at 36-km and 12-km resolution for the full 12-month period, BAMS produced a series of sensitivity tests to determine the optimal meteorological setup for the annual modeling. This paper details the results from this sensitivity testing.

2. DESCRIPTION OF THE METEOROLOGICAL MODELING APPROACH

The meteorological model used in this study is the PSU/NCAR Mesoscale Model (MM5 version 3.6, Grell et al., 1994). In order to build on prior relevant MM5 modeling results funded by the EPA and other RPOs, those studies serve to establish the initial model configuration for this effort. Those findings are summarized in Olerud, 2003a. The modeling results indicate that MM5 is most sensitive to the selection of planetary boundary layer (PBL) and soil schemes. Therefore a series of sensitivity tests are recommended in Olerud, 2003b. Given limited time and budget resources, a series of four sensitivity tests are laid out testing primarily the model response to the selection of PBL scheme and soil model. These are the tests:

1) **px_acm**: Pleim-Xiu land surface model, asymmetric convective mixing PBL (Xiu and Pleim, 2000).
2) **noah_mrf**: Noah land-surface scheme (Chen and Dudhi, 2001) with the medium range forecast (mrf) PBL (Hong and Pan, 1996).
3) **multi_blkdr**: Multi-layer soil scheme with Blackadar PBL and Zilitinkevich thermal roughness length.
4) **noah_eta-my**: Noah land-surface scheme with the ETA Mellor-Yamada PBL (IMVDIF=0).

The common options for all sensitivity tests include Kain-Fritsch 2 cumulus parameterization (Kain and Fritsch, 1993; Kain, 2002), mixed phase (Reisner 1) microphysics (Reisner et al, 1998), and Rapid Radiative Transfer Model (RRTM) radiation (Mlawer et al, 1997). The runs are made with analysis nudging coefficients set as follows (36-km and 12-km resolutions):

Winds (aloft):	2.5E-4,1.0E-4,
Winds (surface):	2.5E-4,1.0E-4,
Temp (aloft):	2.5E-4,1.0E-4,
Temp (surface):	0,0
Moisture (aloft):	1.0E-5,1.0E-5
Moisture (surface):	0,0

Note that the use of the ETA M-Y pbl scheme necessitates moist vertical diffusion being turned off. Figure 1 shows the 36-km and 12-km modeling domains. The runs are executed in 2-way mode with feedback turned off. The four sensitivity runs are executed for three separate episodes listed below:

Episode 1:	Jan 2-21, 2002
Episode 2:	Jul 13-28, 2001
Episode 3:	Jul 13-22, 1999.

* *Corresponding author address*: Donald T. Olerud, Jr., Research Scientist, Baron Advanced Meteorological Systems, 3021 Cornwallis Road, Research Triangle Park, NC, 27709 don.olerud@baronams.com

Each episode is preceded by a spin-up period (7, 7, and 4 days, respectively) that will not be discussed in this report. The runs are made in 5.5-day segments, each starting at 00 UTC, with the first 12 hours of each segment serving as spin-up.

3. EVALUATION APPROACH

It is common in the air quality community to use surface statistics of the base meteorological variables as the dominant metrics to determine acceptable model performance. Often statistics for only temperature, mixing ratio and wind speed are calculated. Obviously it is important for the model to accurately represent these variables, but there are additional variables that also become important when one considers that the results will be used to improve visibility. As such we have added cloud cover, relative humidity, and precipitation to the performance suite. While we calculate metrics separately for wind direction and wind speed, we also calculate the mean error vector as perhaps the single best metric to quantify overall wind performance.

Recognizing that qualitative analyses of the model output are as important as standard quantitative analyses, we enable the systematic visualization of model fields with observations overlaid whenever possible. To do this we process the MM5 output through EPA's MCIP2 program. MCIP2 transforms the data into NetCDF format while also calculating a few fields (e.g. low, middle, and high CFRAC) that are not readily available in the raw MM5 output. MCIP2 also interpolates temperature and wind speed to observation height (1.5m and 10m, respectively) for more accurate evaluation. Even though MCIP2 outputs a total cloud fraction, CMAQ uses this quantity to estimate optical depth. Accordingly its value can be markedly different than what meteorologists typically regard as cloud fraction. To make things as consistent as possible between the model and observations, the cloud fractions presented in this report represent the maximum of the low, middle, and high cloud fractions. We also use MCIP2 to cull a minimum of six cells about the domain periphery to minimize edge effects. The reduced domain precisely matches the domain used in the air quality modeling. The 36-km analysis domain thus contains 148 columns, 112 rows, and 34 layers. The 12-km analysis domain covers 168 columns, 177 rows, and 34 layers.

The observations used for statistics come primarily from UCAR's ds472.0 (TDL) archive (http://dss.ucar.edu/datasets/ds472.0/). These data are quality controlled and converted to NetCDF format, thus allowing the data to be visualized on the model fields via PAVE (http://www.cep.unc.edu/empd/EDSS/pave_doc/index.shtml). Unfortunately the precipitation values in this dataset are not reliable, so we calculate precipitation statistics based on the 24-h gridded accumulations available from the Climate Prediction Center (CPC) (http://www.cpc.ncep.noaa.gov/products/precip/realtime/retro.html). These fields, originally at 0.25-degree resolution, undergo grid transformation to match our 36-km and 12-km domains. Since the CPC analyses are derived primarily from rain gauges, the statistics are only calculated over cells that MM5 deems to be land.

For aloft analyses we process standard sounding observations from the NCEP ds353.4 archive (http://dss.ucar.edu/datasets/ds353.4/). These observations are quality controlled and used to produce model/observation skewT sounding plots for selected sites. Additionally we integrate the observations into sigma levels that match the MM5 specifications, after which we can statistically analyze performance at sigma levels 9, 17, and 22 (~500m, ~1600m, ~3400m, respectively). Qualitative profiler plots showing model/observed hourly winds are also created based upon the data stored at the Forecast Systems Lab (http://www.profiler.noaa.gov/jsp/). These results, along with much more, will not be presented here. The reader is referred to the VISTAS meteorological website (http://www.baronams.com/projects/VISTAS/) for additional evaluation details and results.

The number of analysis plots available on the above website is truly daunting. To aid in performing cross-sensitivity analyses, data are summarized by averaging over four hours (7-10 UTC or 18-21 UTC) or over an entire day. The resultant PAVE plots are arranged in a 4-panel presentation allowing quick qualitative comparison between sensitivities. For statistical comparison we have created cross-sensitivity time series plots of key model statistics, namely bias, error, and index of agreement.

Our statistical analyses involve additional parsing of the data. Figure 2 shows the observing sites color-coded by RPO. Statistics are calculated and stored at each observing site, and we routinely aggregate these results to produce statistical time series plots and tables for every appropriate RPO region. This approach also enables us to produce station-specific statistical quantities that can be plotted in a similar manner to Figure 2. The VISTAS web page even shows an animation of how these quantities change throughout an episode-composite day. The results shown in this document focus on statistics aggregated only over the VISTAS portion of the 12-km domain.

4. RESULTS

The initial results for the px_acm run for episode 1 were quite discouraging. The run showed a significant cold bias over much of the eastern US, including the VISTAS region as illustrated in figure 3. While mixing ratio, clouds, precipitation, and winds were modeled reasonable well, the large cold bias was unexpected based on prior findings from other RPO's and the EPA. Note in figure 3 that the first couple of days showed very little temperature bias, but the bias increased as the mean temperature rose. After much investigation it became apparent that the deep soil temperature was initiated during an extreme cold event in the eastern US. Since the model soil temperatures and moisture were passed from one model segment to another via the interppx preprocessor, the cold soil acted as a continuous drag on the atmosphere that the model physics could never quite overcome.

The bias problem is significantly reduced by simply running each model segment independently, thus limiting the cold drag to actual cold conditions. Figure 4 shows the statistical time series for this new case, dubbed px_acm2. The summer episodes do not suffer from this cold bias initialization effect. For the cross-sensitivity analyses that follow, therefore, px_acm2 will replace px_acm only for episode 1.

Figure 5 shows the daytime PBL heights for January 10, 2002 at 12-km resolution over the VISTAS region. It should be noted that the noah_eta-my PBL heights can erroneously become negative over small spatial areas; we set all such negative values to zero before averaging. Due to the small areal extent of these negative PBL values, we do not anticipate any qualitative assessments to be affected by those artifacts. The January 10, 2002 PBL heights are rather typical of winter PBL heights. The noah_mrf heights are significantly higher and smoother than those in the other sensitivities. Generally speaking, the noah_eta-my daytime PBL heights are lower than they are in the other sensitivity runs. The px_acm2 heights tend to be more in the middle of those extremes, though they also "bottom out" more than the other runs.

Figure 6 shows the cross-sensitivity daytime precipitation plot for this same day. The low PBL heights in the px_acm2 run are closely correlated to precipitation in the Ohio Valley, while melting snow and clouds (figure 7) might inhibit mixing over the northern Mid-Atlantic States.

Figure 8 shows the daily average temperature for this same day. Note that the px_acm2 case is generally warmer than the other cases, while the noah_eta-my run is the coldest. Figure 9 shows that for daily averaged mixing ratio the patterns are very similar for all runs. The combination of warmer daytime temperatures and similar mixing ratios results in lower daytime relative humidity for the px_acm2 case compared with the other sensitivity runs (figure 10). Finally, figure 11 shows that the daytime wind speeds are similar in all cases.

Traditionally nighttime PBL heights have not been considered very important for air quality modeling, but visibility/particulate modeling has changed that paradigm. Figure 12 shows the nighttime (07-10 UTC) PBL heights for January 10, 2002. Notice that the px_acm2 produces lower PBL heights than the rest of the sensitivity cases do, thus trapping surface-based emissions in a smaller volume of air than would occur in another MM5 configuration. The noah_mrf run again produces the highest PBL heights at night, while the multi_blkdr and noah_eta-my runs are somewhere in the middle.

Nighttime cloud cover is shown in figure 13. The most striking observation from this figure is the cloud deck over Tennessee in the noah_eta-my run that does not exist to the same extent in the other sensitivity runs.

Figure 14 shows the nighttime relative humidity plot. One might expect that the px_acm2 case would show the highest relative humidity, given the low PBL heights as indicated by figure 12. The opposite is actually the case. The warmer temperatures in this run counteract the increased stability such that the relative humidity values are the lowest of all the runs. The noah_eta-my run easily exhibits the highest relative humidity.

Figure 15 shows the nighttime wind speed. Speeds are lowest in the noah_eta-my run, followed by px_acm2, noah_mrf, and multi_blkdr. In fact, the latter two cases seem to show an inappropriate diurnal pattern in that their nighttime wind speeds are higher than their daytime wind speeds (figure 12).

Many of the same observations reported above are also valid for the summer episodes. To save time we will only show spatial 4-panel plots for PBL heights for a sample summer day, July 19, 2001. Figure 16 shows the daytime average, while figure 17 shows the nighttime average.

Now that a qualitative understanding of these sensitivity runs has been established, the remainder of this report will focus on quantitative comparisons between the sensitivity cases. Figure 18 shows the temperature statistical time series plot for episode 1. While the general performance of the model is very similar across the sensitivity runs, close examination reveals that the px_acm2 case performs the best.

Figure 19 shows the corresponding plot for episode 2. The noah_eta-my run clearly performs the worst, while the sensitivity runs show similar performance. The episode 3 plot (not shown) reveals similar responses.

Figure 20 shows the 12-km mixing ratio statistical time series plot for episode 1 over the VISTAS region. Overall the noah_mrf case performs the best, followed by px_acm2. The multi_blkdr case is clearly the poorest performing. The corresponding episode 2 plot (figure 21) reveals a different result in that the noah_mrf case is negatively biased in mixing ratio. This weakness presumably stems from dry air being mixed down from aloft as the PBL becomes too high. The other cases are relatively similar. The negative mixing ratio bias is also evident for noah_mrf in episode 3 (not shown).

The wind direction plot for episode 1 is shown in figure 22. The direction bias and error plots show similar performance among the sensitivity cases, but the magnitude of the error vector plot (bottom panel) shows that the noah_eta-my is the best performing run, especially at night. The px_acm2 run is generally second best. Figure 23 shows that similar results are seen in episode 2, as well as in episode 3 (not shown).

The cloud cover statistical plots (figures 24-25) show very little difference in performance among the sensitivity runs. Figure 26 reveals that relative humidity for episode 1 is best modeled by either px_acm2 or noah-mrf, with the multi_blkdr case performing the worst. The episode 2 plot (figure 27) shows a strong diurnal signature with the sensitivity runs generally being negatively biased at night and positively biased during the day. The diurnal signature is interestingly the weakest for the noah_eta-my run, leading to that sensitivity possibly performing the best for this quantity. The episode 3 plot (not shown) has the noah_eta-my run displaying the poorest performance, no doubt due to its negative temperature bias.

Figure 28 shows the precipitation statistics for the full 12-km grid for episode 1. The bias blip on January 10 resulted from there being very few grid cells that actually observed measurable precipitation on that day. Sensitivity px_acm2 clearly outperforms the other cases for this episode. Figure 29 shows the corresponding plot for episode 2. Sensitivity noah_eta-my seems to be relatively unbiased, while the other sensitivity runs show a slight low bias. Nevertheless the skill plots show little difference in performance among the runs. The px_acm case appears to show slightly better results than do the other runs. Similar results are found for episode 3 (not shown).

Figure 30 is designed to show which sensitivity case statistically performs the best at each valid observation site. This particular image represents a composite of 1.5m temperatures for all hours, with absolute error being the defining metric. Note that the px_acm2 run performs best for a majority of the sites. The noah_eta-my run appears to do quite well over Florida. Figure 31 shows the corresponding plot for episode 2. Again the px_acm case seems to perform best overall, though noah_eta-my again performs best in Florida and along the southeastern coastline. The results for episode 3 (not shown) reveal no best performing sensitivity.

Figure 32 shows a similar type of plot for mixing ratio. The noah_mrf case appears to perform best for the largest number of sites, followed by the px_acm2 case. The episode 2 results (figure 33) indicate just the opposite, as the noah_eta-my or multi_blkdr cases seem to perform best for most of the sites. The episode 3 plot (not shown) is a mixed bag with the noah_eta-my and px_acm cases seemingly performing best.

The corresponding series of plots for the magnitude of the error wind vector (figures 24-35) show the clear superiority of the noah_eta-my runs. The px_acm(2) runs perform a distant second best for all sensitivities. The main reason why noah_eta-my performs so well is its ability to calm its wind speeds at night (figure 15) relative to the other model configurations.

5. DISCUSSION

After this rather exhaustive quantitative and qualitative assessment of four sensitivity runs over three episodes, the px_acm(2) runs appear to perform the best overall. While statistical performance for px_acm(2) for certain quantities might be surpassed by other model configurations (e.g. noah_eta-my winds), it seldom performs the poorest of the four sensitivities tested.

A few general conclusions can be drawn about these sensitivity tests. They are:

1) PBL heights are consistently highest in the noah_mrf simulations, while the noah_eta-my runs consistently produce the lowest daytime PBL heights. At night the px_acm(2) PBL heights are usually lowest.
2) Surface winds are consistently best represented by the noah_eta-my runs, in large part because that configuration appropriately produces the calmest winds at night.
3) The px_acm2 temperatures are modeled better than all other configurations for the winter episode, including px_acm. The noah_eta-my

runs consistently show the most extreme low temperature bias of all configurations for all episodes.

4) All configurations other than noah_eta-my exhibit similar performance in modeling measurable 24-h precipitation. The noah_eta-my runs produce more precipitation coverage and are generally slightly less skilled than the other sensitivities, especially for the winter episode.

The px_acm configuration was anticipated to perform the best, and in many ways it has. However the noah_eta-my configuration is very intriguing. It consistently shows the best wind performance at the surface, despite suffering from the most severe negative temperature bias. In the summer it also appears to be the least biased in terms of precipitation. Its daytime PBL heights appear to be a little lower than reality, but there are no observations available to support that conjecture. Statistics that are calculated for layers ~500m, ~1600m, and 3400m (not shown) reveal very little statistical difference aloft among the sensitivities, with the occasional exception of degraded performance for the noah_mrf runs (PBL too high?) and noah_eta-my (PBL too low?).

Still, the superior surface wind performance of the noah_eta-my run deserves additional attention. To compare the performance of this run versus px_acm(2), we computed composite statistics at various sounding locations. These statistics considered only the 00 UTC (or 12 UTC) data in the composite. A plot of this type is shown in figure 36 for Greensboro, NC, episode 1, 00 UTC. Note that at the surface the wind errors are less in the noah_eta-my case than they are in the px_acm2 case, but for the majority of the lower portions of the atmosphere the opposite occurs. The large temperature/dew point biases/errors in the noah_eta-my are expected and corroborate what is seen in the surface statistics. Figure 37 shows that for this site similar results are found in the wind profile for a summer episode.

Given these findings, the recommended approach for annual MM5 modeling in support of VISTAS is to use the px_acm2 approach. Additional testing (not shown) reveals that running a px_acm2 configuration for the summer episodes provides similar performance to the px_acm runs. In the winter px_acm2 clearly outperforms px_acm for episode 1, thus making it the single best option overall.

ACKNOWLEDGEMENTS

The authors would like to thank Sylvain Dupont for his patient assistance in getting the MPP version of PX working. We also thank Dr. Jack Kain for providing us with an MPP-ready version of the Kain-Fritsch 2 cumulus parameterization. The authors appreciate the able assistance Steve Thorpe providing in helping to get MM5-MPP working on the MCNC Center for Networked Information Discovery and Retrieval (CNIDR) Linux cluster.

REFERENCES

Chen, F., and J. Dudhia, 2001: Coupling an advanced land-surface/hydrology model with the Penn State/NCAR MM5 modeling system. Part I: Model implementation and sensitivity. Mon. Wea. Rev., 129, 569-585.

Chen, F., and J. Dudhia, 2001: Coupling an advanced land-surface/hydrology model with the Penn State/NCAR MM5 modeling system. Part II: Preliminary Model validation. Mon. Wea. Rev., 129, 587-604.

Grell, G. A., J. Dudhia, and D. R. Stauffer, 1994: A description of the fifth-generation Penn State/NCAR Mesoscale Model (MM5). NCAR Tech. Note, NCAR/TN-398+STR, 122 pp.

Hong, S.-Y., and H.-L. Pan, 1996: Nocturnal boundary layer vertical diffusion in a medium range forecast model, *Mon. Wea. Rev,,* **124**, 2322-2339.

Kain, J. S. and J. M. Fritsch, 1993: Convective parameterization for mesoscale models: The Kain-Fritsch scheme, *The Representation of Cumulus Convection in Mesoscale Models,* K. A. Emanuel and D. J. Raymond, Eds., American Meteorological Society, Boston, 246 pp.

Kain, John S., 2002: The Kain-Fristch convective parameterization: An update. To be submitted to J. of Appl. Meteoro.

Mlawer, E. J., S. J. Taubman, P. D. Brown, M. J. Iacono, and S. A. Clough, 1997: Radiative transfer for inhomogeneous atmospheres: RRTM, a validated correlated-k model for the longwave. J. Geophys. Res., 102(D14), 16,663-16,682.

Olerud, D. T., 2003: Summation of Relevant MM5 Sensitivity Modeling in Support of VISTAS (Visibility Improvement - State and Tribal Association), VISTAS task 2a deliverable. Available from Mike Abraczinskas, Meteorologist, NC Division of Air Quality, 1641 Mail Service Center, Raleigh, NC 27699-1641

Olerud, D. T., 2003: Recommended MM5 Sensitivity Modeling in Support of VISTAS (Visibility

Improvement - State and Tribal Association)] VISTAS Task 2b deliverable. Available from Mike Abraczinskas, Meteorologist, NC Division of Air Quality, 1641 Mail Service Center, Raleigh, NC 27699-1641

Reisner, J., R. M. Rasmussen, and R. T. Bruintjes, 1998: Explicit forecasting of supercooled liquid water in winter storms using the MM5 mesoscale model. Quart. J. Roy. Metero. Soc., 124 B, 1071-1107.

Xiu, A., and J.E. Pleim, 2000: Development of a land surface model. Part I: Application in a mesoscale meteorology model. Journal of Applied Meteorology, 40, 192-209.

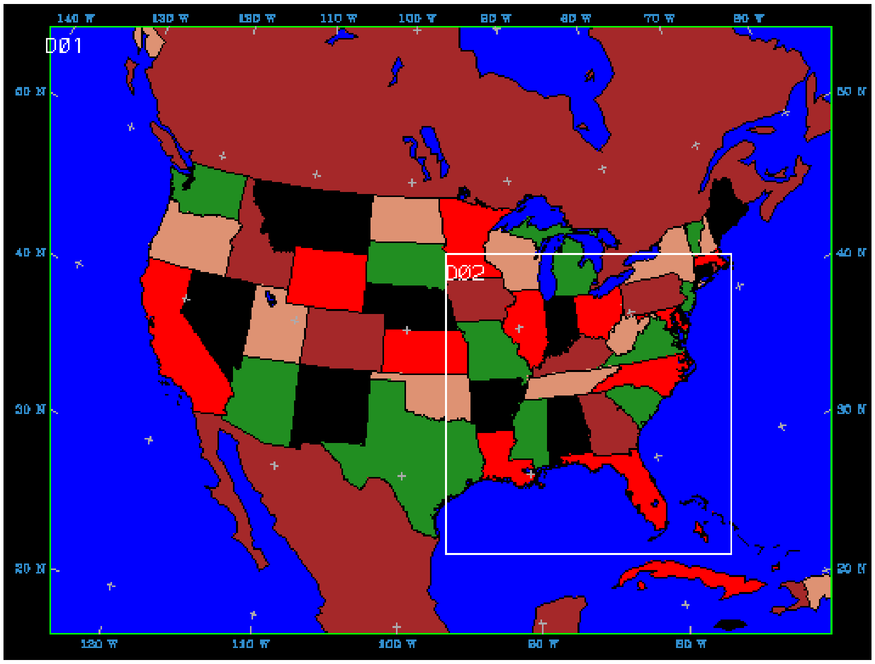

Figure 1. VISTAS 36-km/12-km MM5 modeling domain

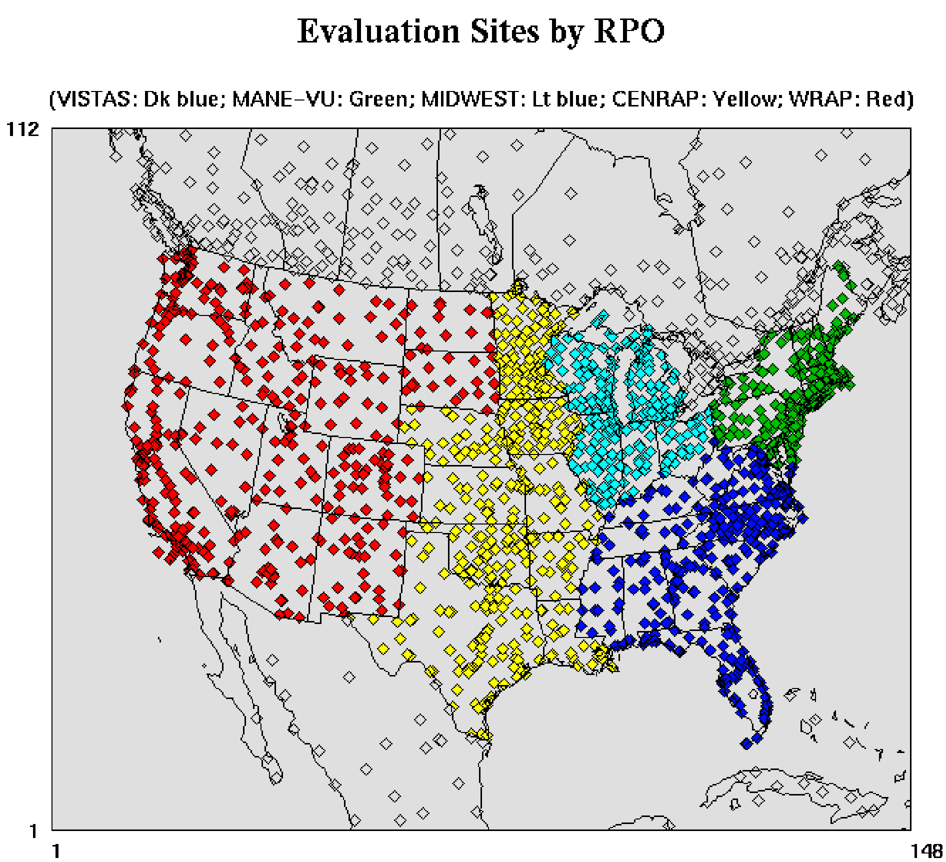

Figure 2. Surface observing network color-coded to represent Regional Planning Organization areas.

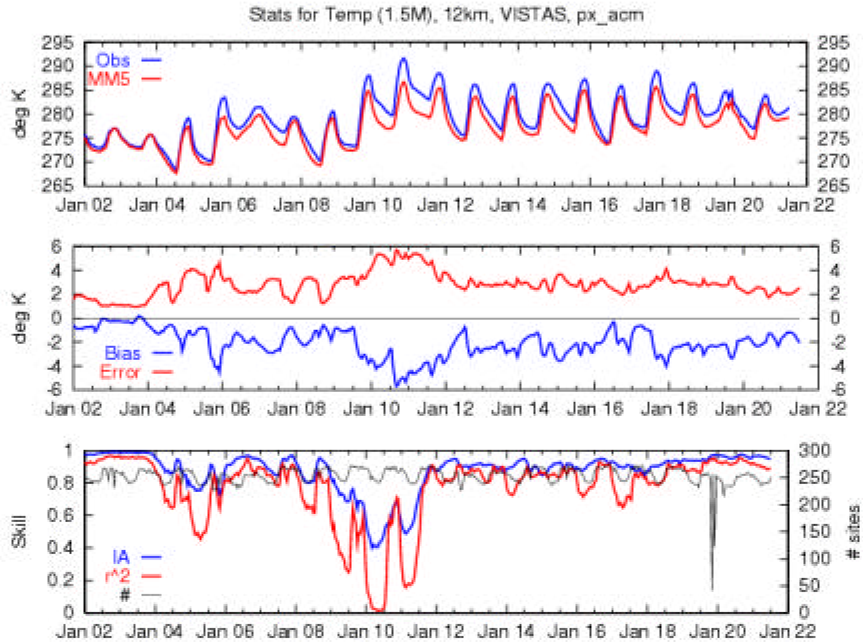

Figure 3. Episode 1 temperature (1.5 m) statistical time series plot for the 12-km VISTAS region, px_acm sensitivity. The top panel shows the mean of the observations (blue) and the model (red), the middle plot shows the model bias (blue) and the absolute error (red), while the bottom plot shows the index of agreement (blue) and coefficient of determination (red).

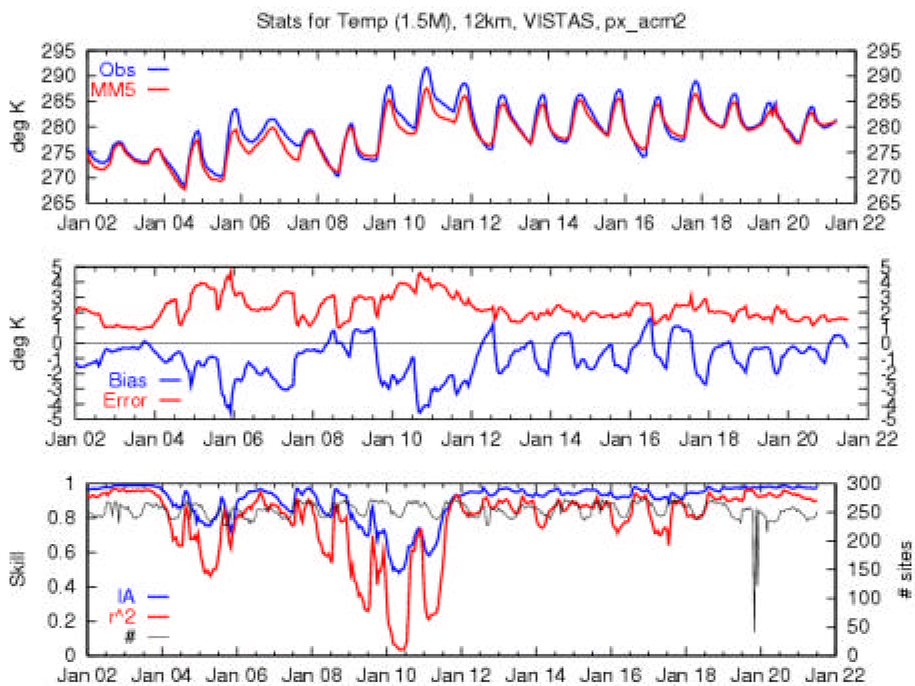

Figure 4. Episode 1 temperature (1.5 m) statistical time series plot for the 12-km VISTAS region, px_acm2 sensitivity. The top panel shows the mean of the observations (blue) and the model (red), the middle plot shows the model bias (blue) and the absolute error (red), while the bottom plot shows the index of agreement (blue) and coefficient of determination (red).

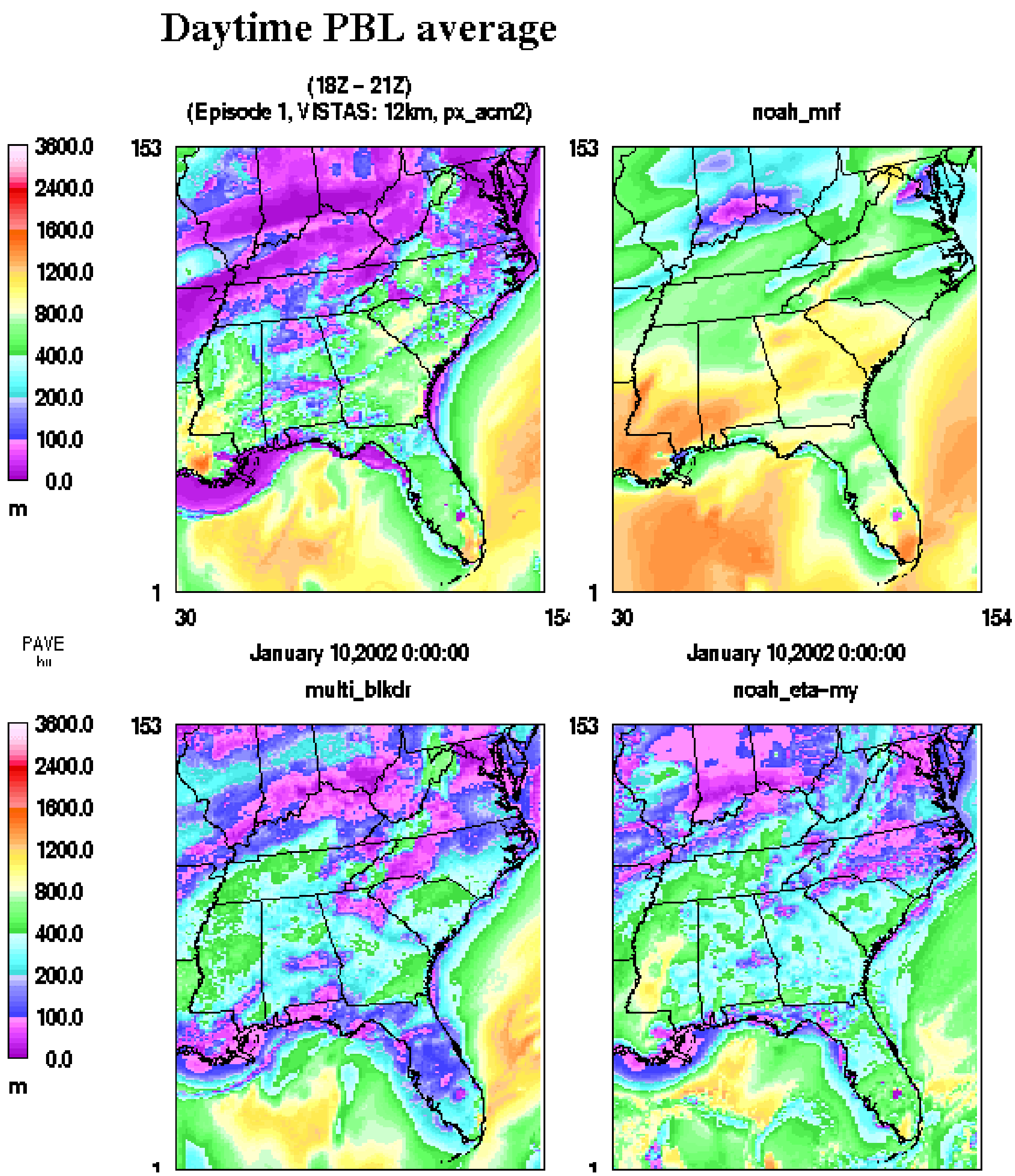

Figure 5. Daytime (18-21 UTC) average PBL heights for the 12-km VISTAS region for January 10, 2002 are displayed. The px_acm2 sensitivity is shown in the upper left, the noah_mrf in the upper right, the multi_blkdr in the lower left, and the noah_eta-my in the lower right. Note that the time value (0:00:00) is only a placeholder and has no physical meaning.

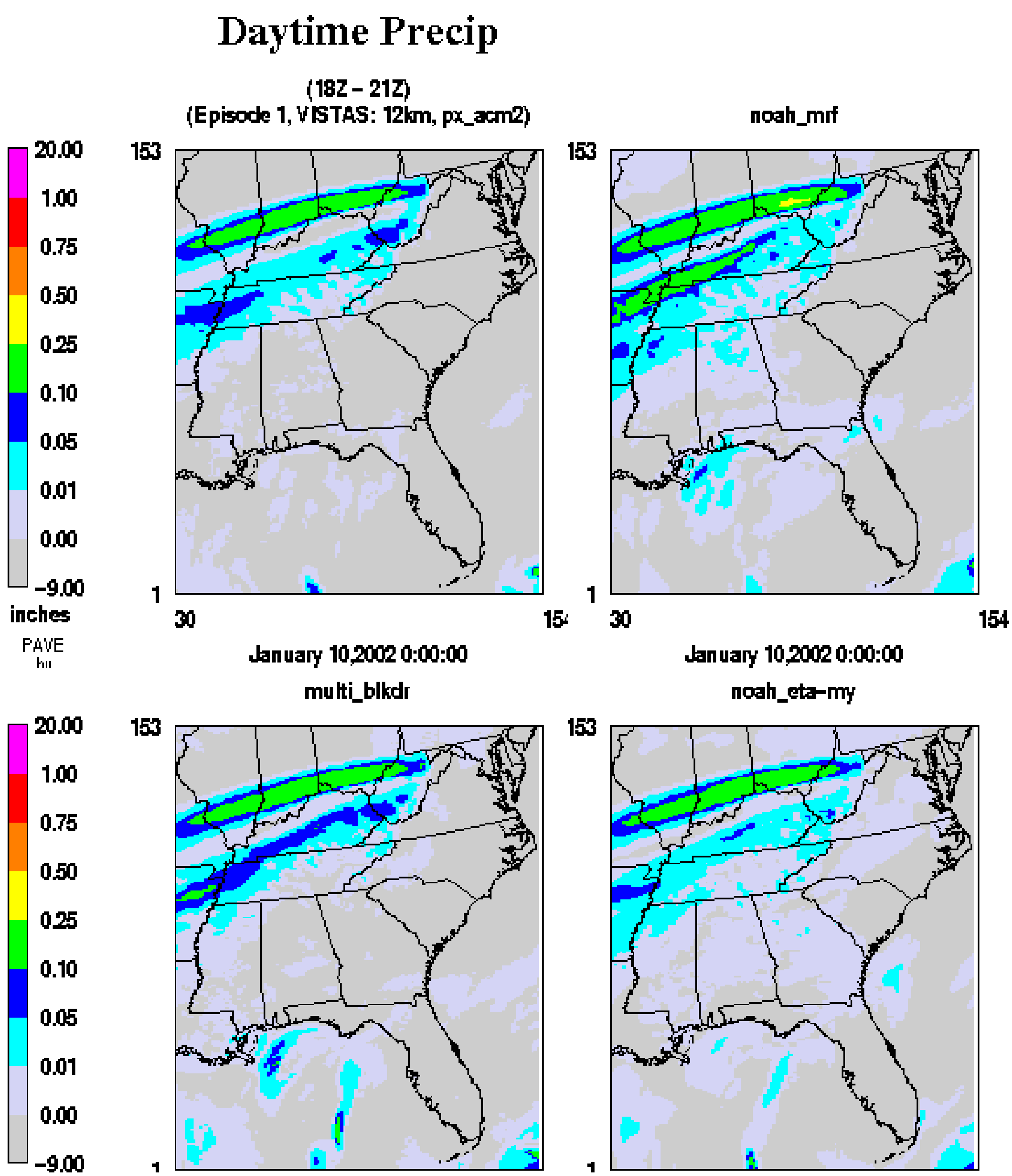

Figure 6. Like figure 5, except for precipitation.

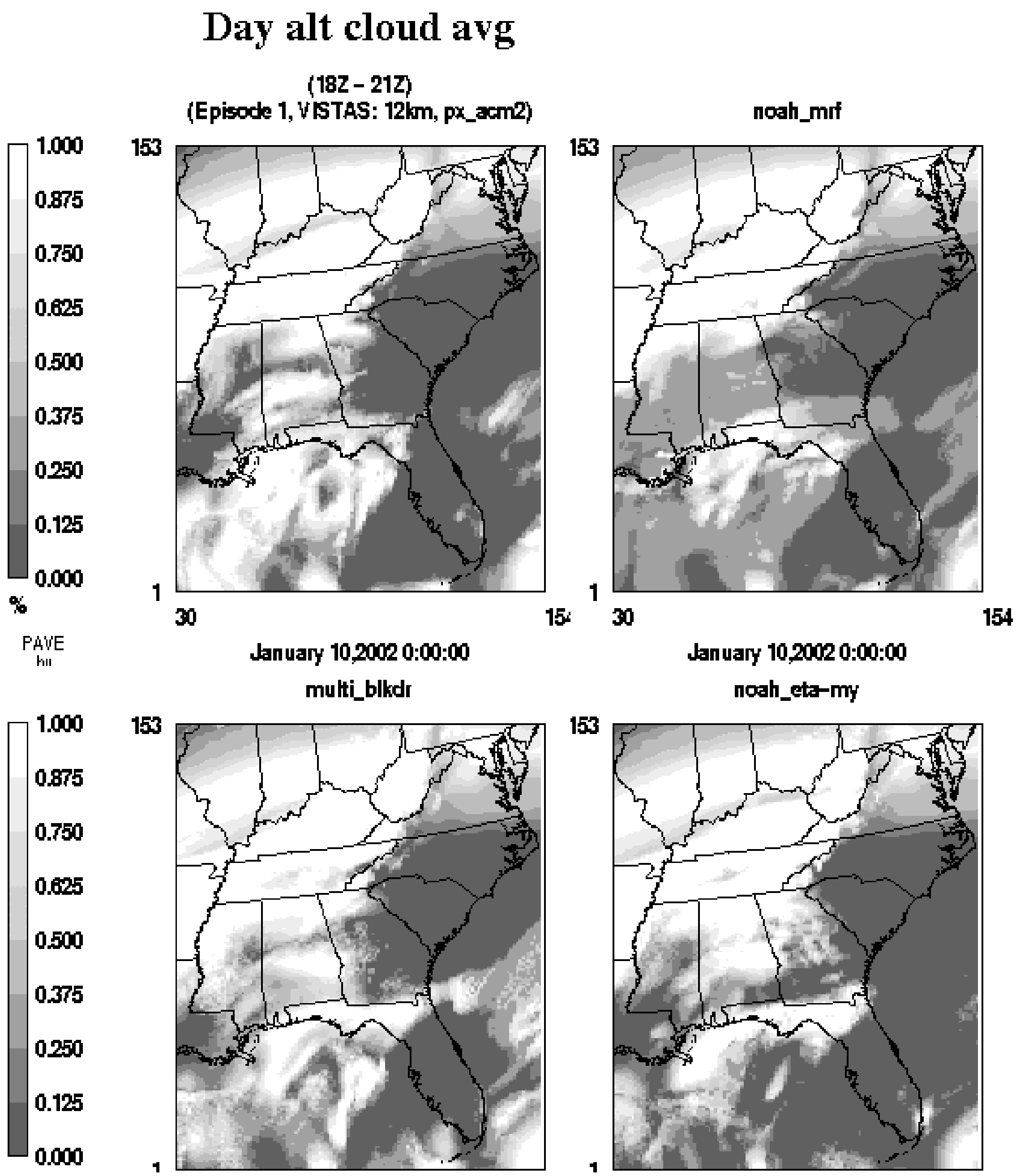

Figure 7. Like figure 5, except for cloud coverage.

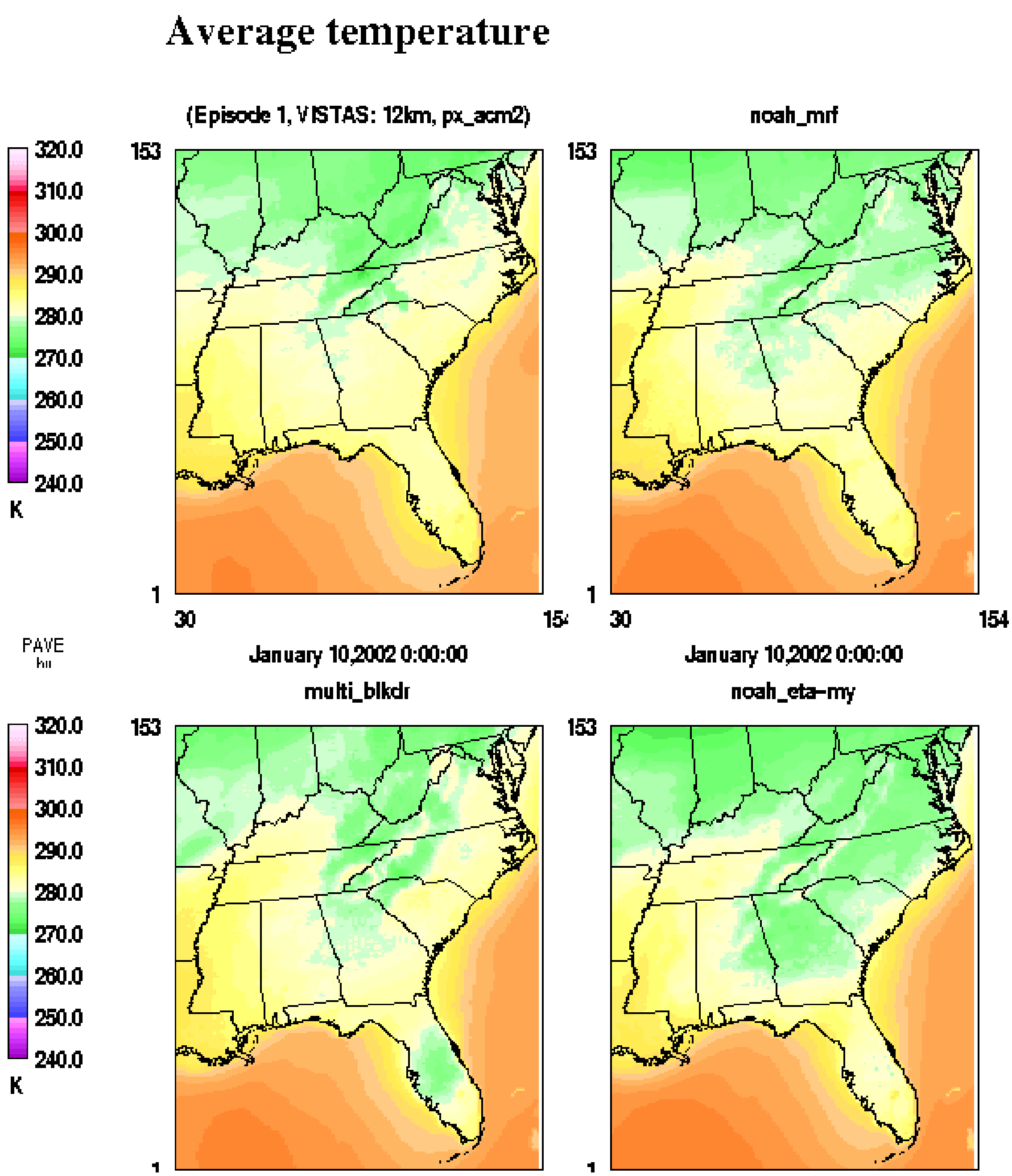

Figure 8. Like figure 5, except for daily average temperature.

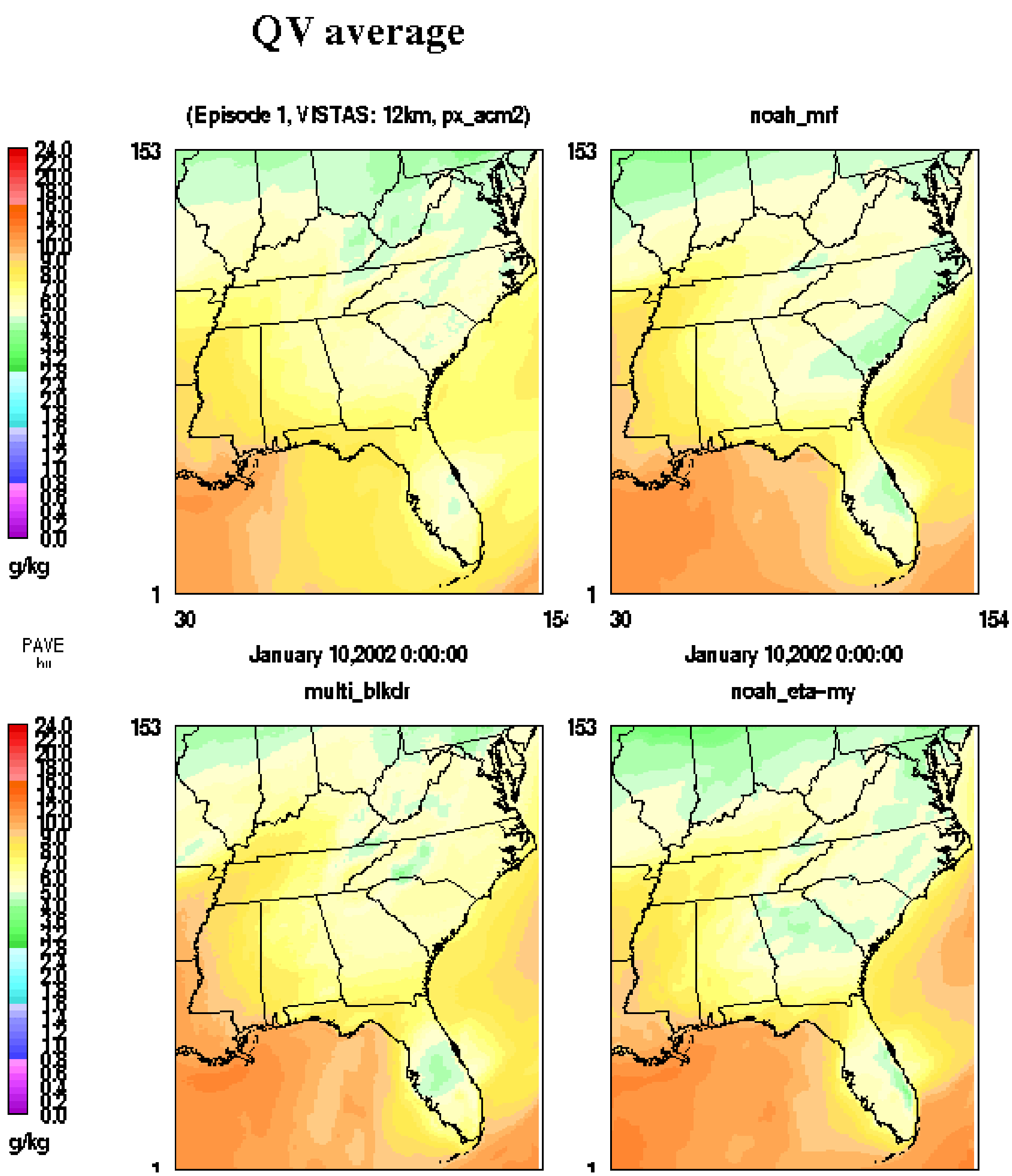

Figure 8. Like figure 5, except for daily average temperature.

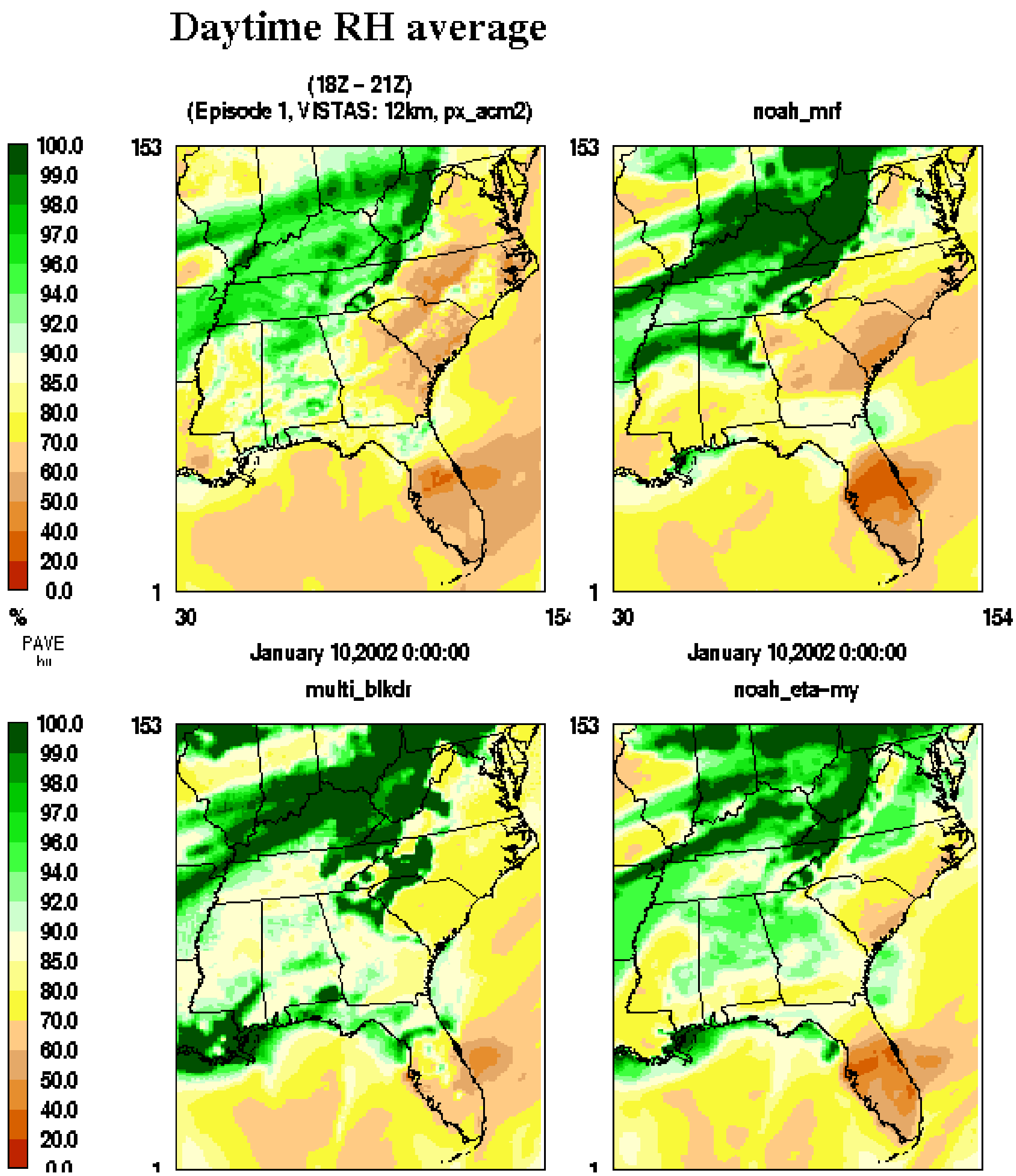

Figure 10. Like figure 5, except for relative humidity.

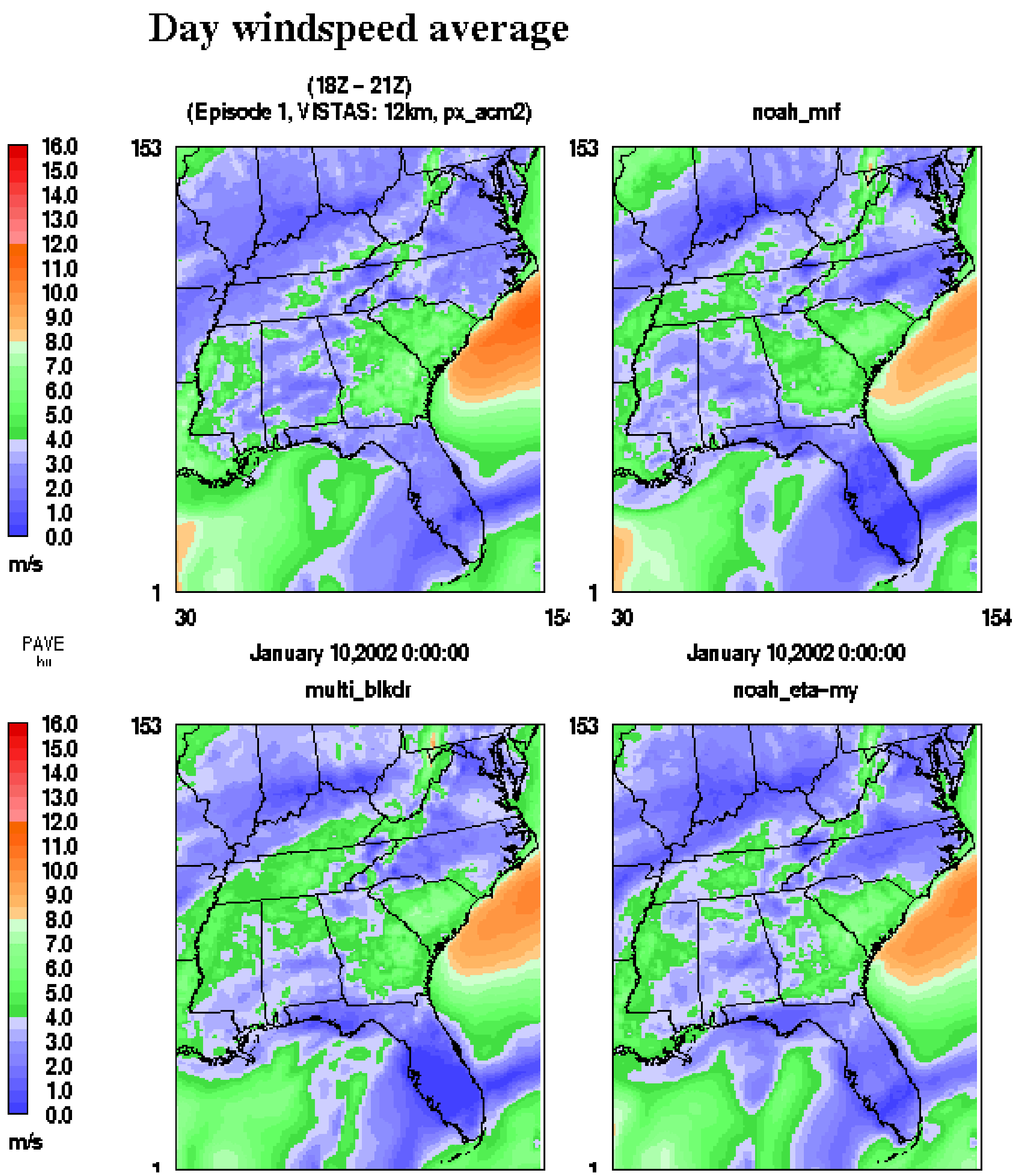

Figure 11. Like figure 5,except for wind speed.

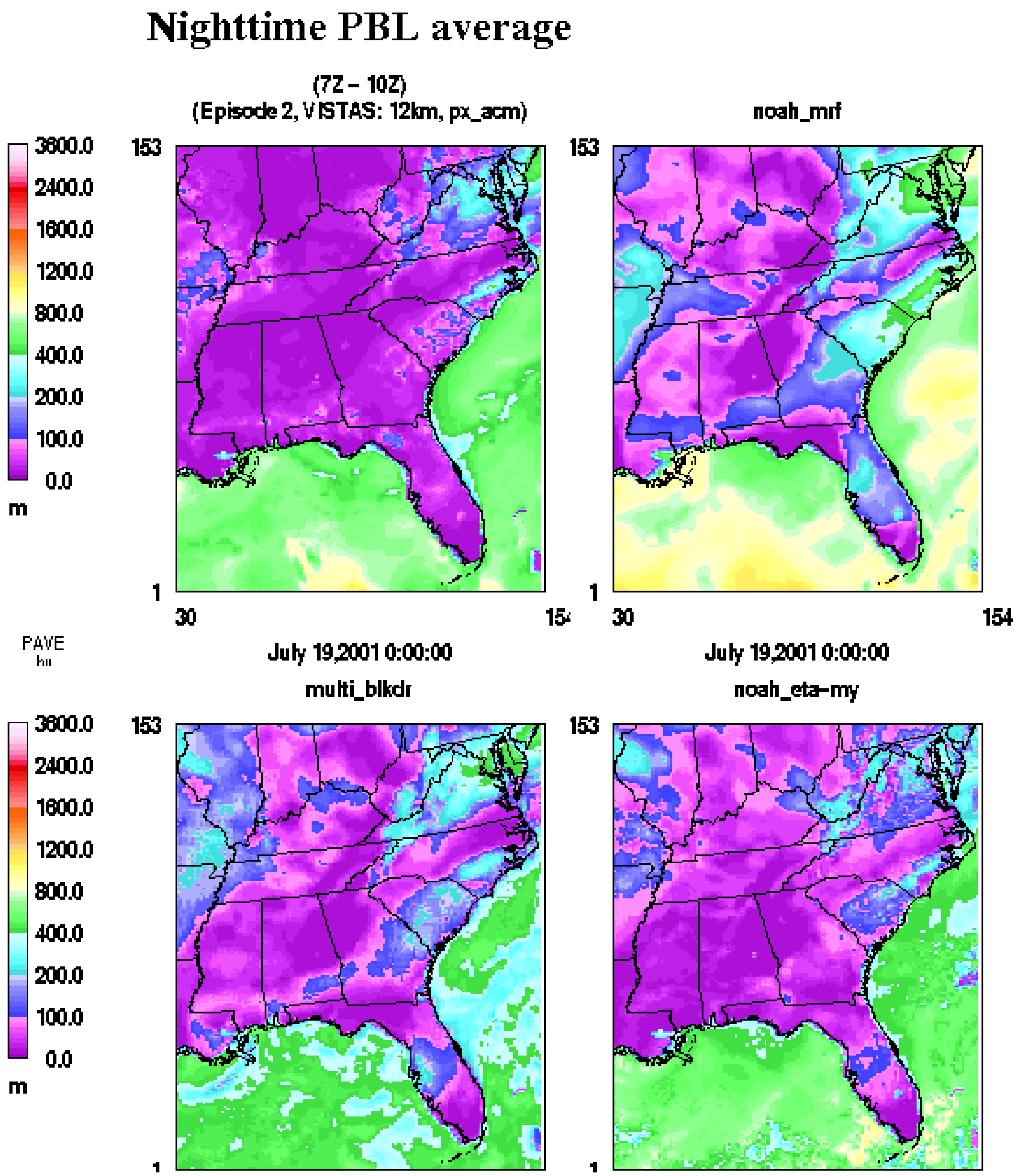

Figure 12. Nighttime (07-10 UTC) average PBL heights for the 12-km VISTAS region for January 10, 2002 are displayed. The px_acm2 sensitivity is shown in the upper left, the noah_mrf in the upper right, the multi_blkdr in the lower left, and the noah_eta-my in the lower right. Note that the time value (0:00:00) is only a placeholder and has no physical meaning.

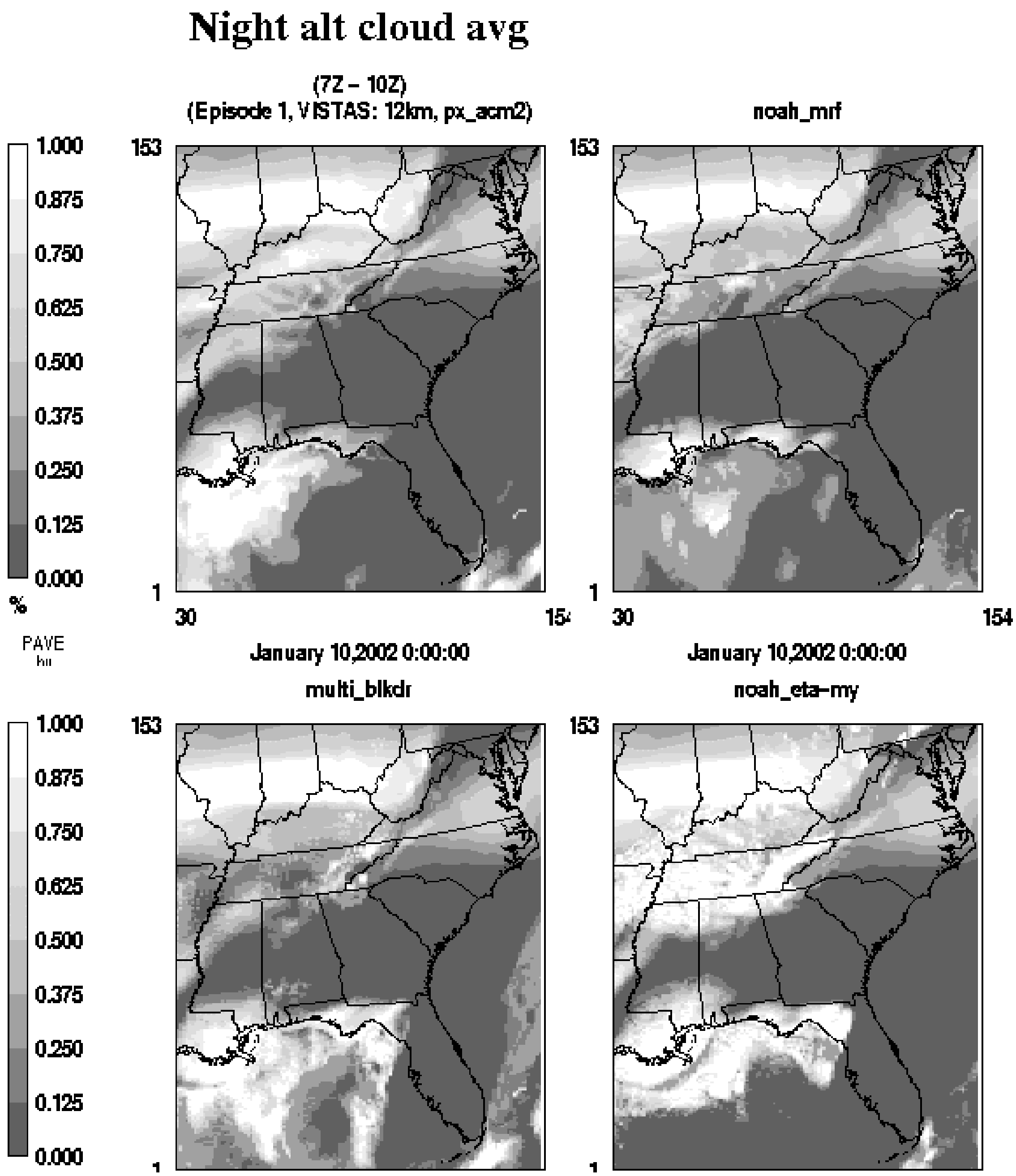

Figure 13. Like figure 12, except for cloud cover.

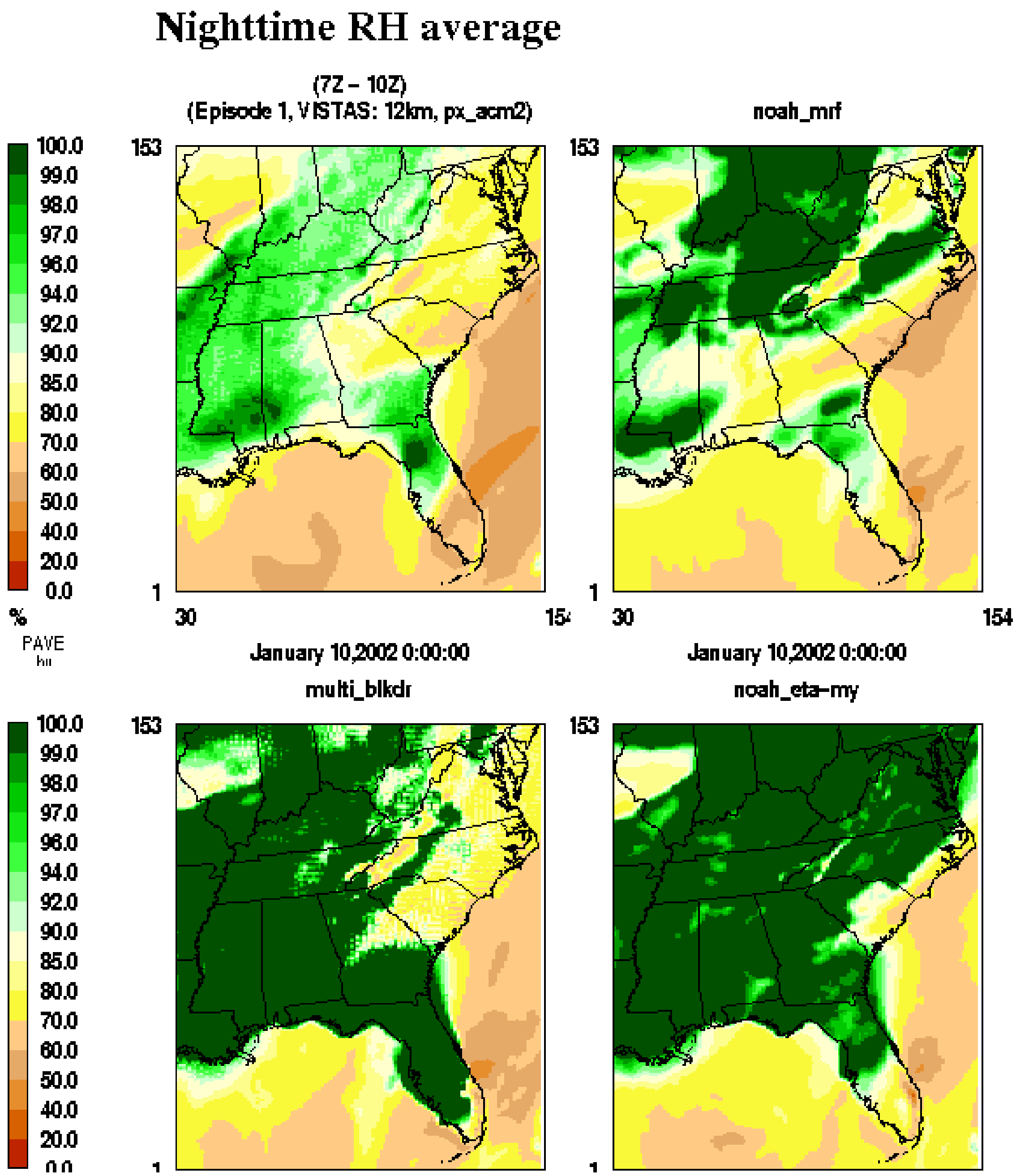

Figure 14. Like figure 12, except for relative humidity.

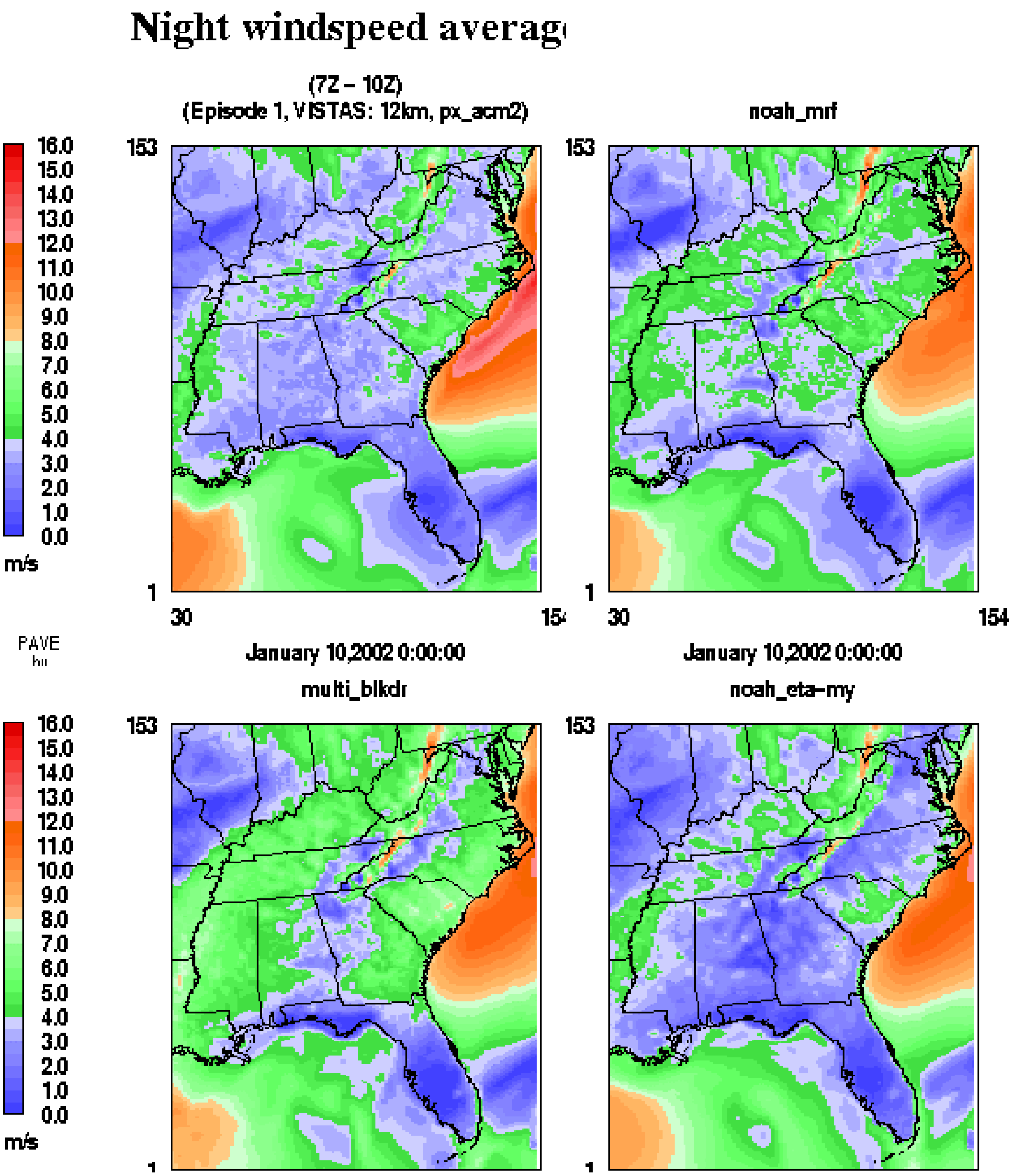

Figure 15. Like figure 12, except for wind speed.

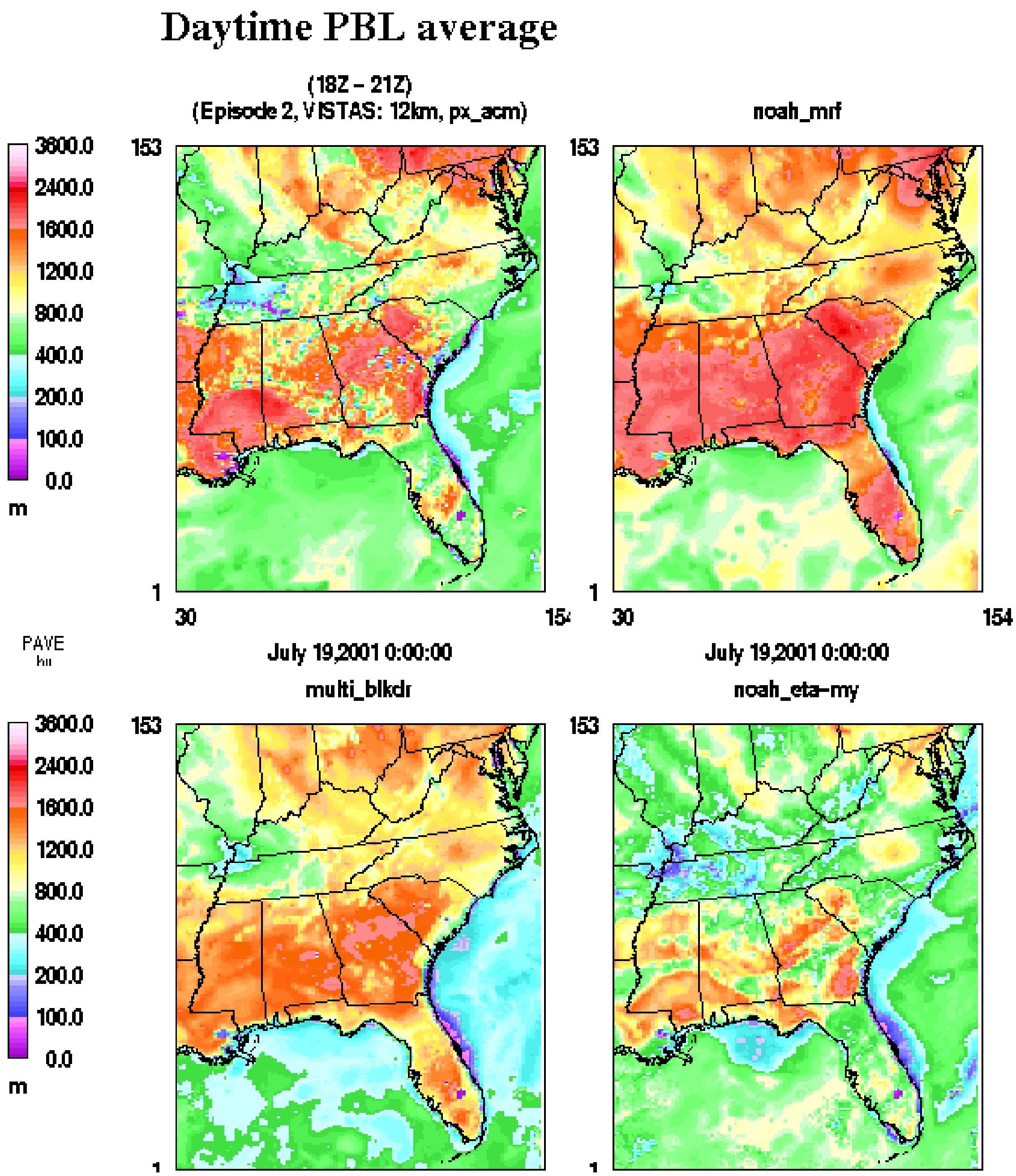

Figure 16. Daytime (18-21 UTC) average PBL heights for the 12-km VISTAS region for July 19, 2001 are displayed. The px_acm sensitivity is shown in the upper left, the noah_mrf in the upper right, the multi_blkdr in the lower left, and the noah_eta-my in the lower right. Note that the time value (0:00:00) is only a placeholder and has no physical meaning.

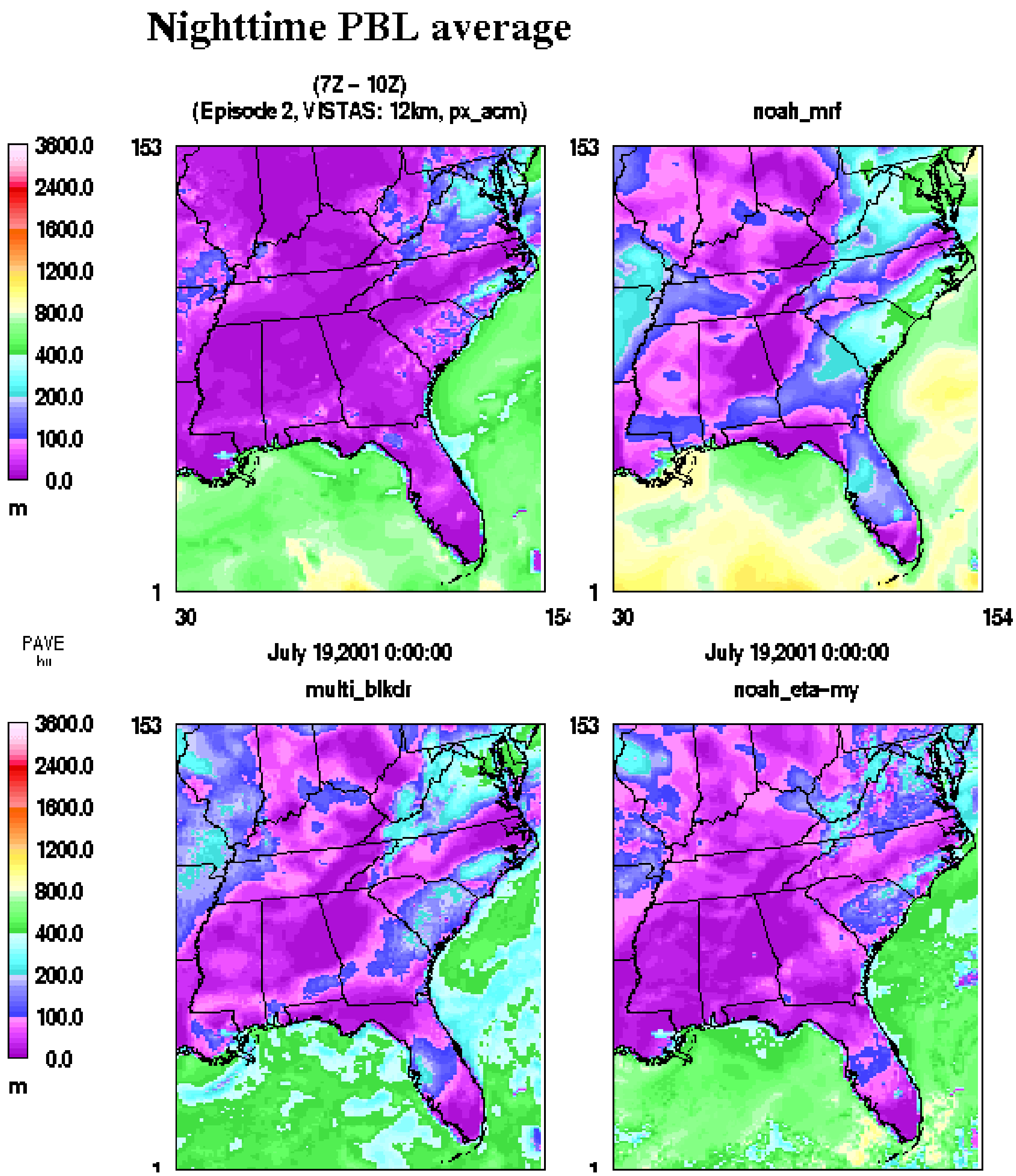

Figure 17. Nighttime (07-10 UTC) average PBL heights for the 12-km VISTAS region for July 19, 2001 are displayed. The px_acm sensitivity is shown in the upper left, the noah_mrf in the upper right, the multi_blkdr in the lower left, and the noah_eta-my in the lower right. Note that the time value (0:00:00) is only a placeholder and has no physical meaning.

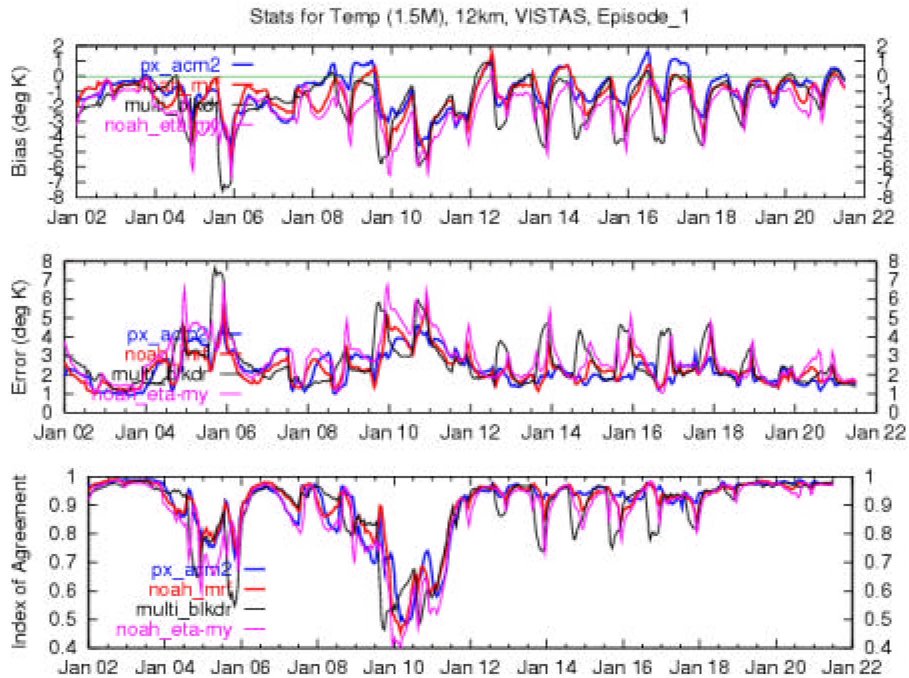

Figure 18. Episode 1 (Jan 2-21, 2002) cross-sensitivity statistical time series plot for temperature is shown. The top panel shows bias, the second panel absolute error, and the bottom panel index of agreement. The px_acm2 case is shown in blue, noah_mrf in red, multi_blkdr in black, and noah_eta-my in purple.

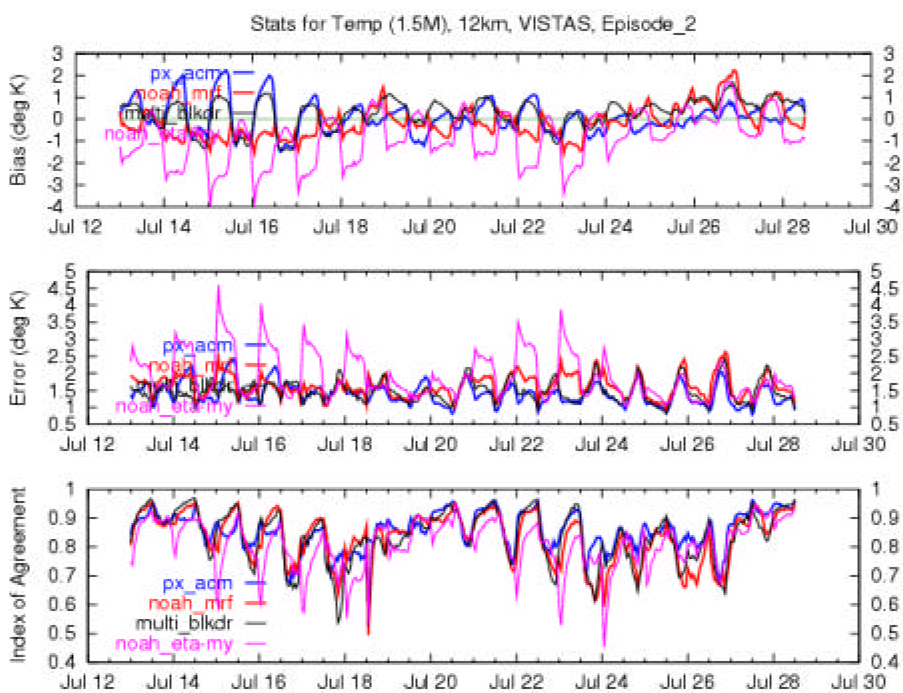

Figure 19. Episode 2 (Jul 13-28, 2002) cross-sensitivity statistical time series plot for temperature is shown. The top panel shows bias, the second panel absolute error, and the bottom panel index of agreement. The px_acm case is shown in blue, noah_mrf in red, multi_blkdr in black, and noah_eta-my in purple.

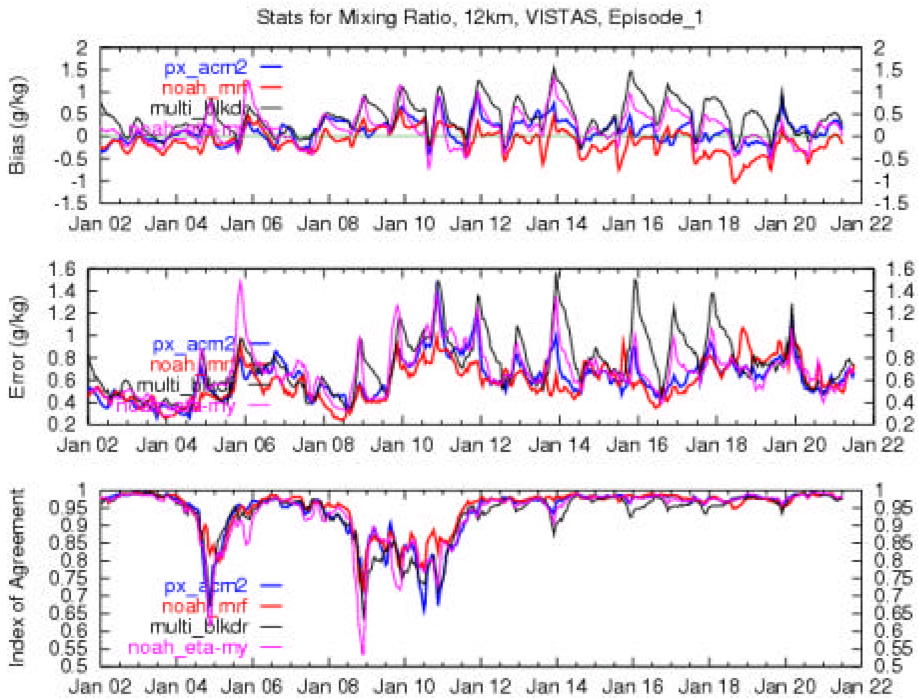

Figure 20. Episode 1 (Jan 2-21, 2002) cross-sensitivity statistical time series plot for mixing ratio is shown. The top panel shows bias, the second panel absolute error, and the bottom panel index of agreement. The px_acm2 case is shown in blue, noah_mrf in red, multi_blkdr in black, and noah_eta-my in purple.

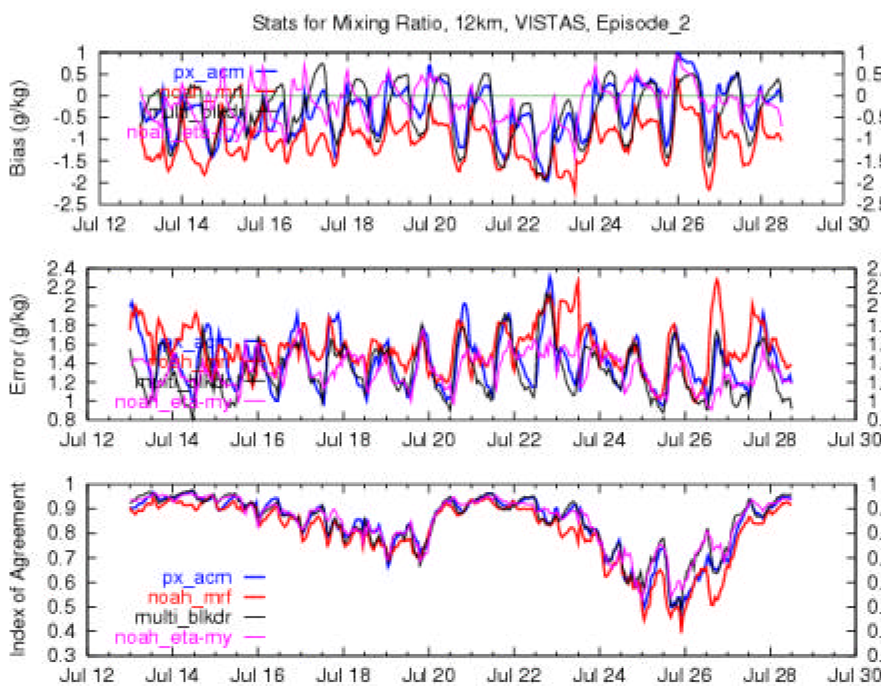

Figure 21. Episode 2 (Jul 13-28, 2002) cross-sensitivity statistical time series plot for mixing ratio is shown. The top panel shows bias, the second panel absolute error, and the bottom panel index of agreement. The px_acm case is shown in blue, noah_mrf in red, multi_blkdr in black, and noah_eta-my in purple.

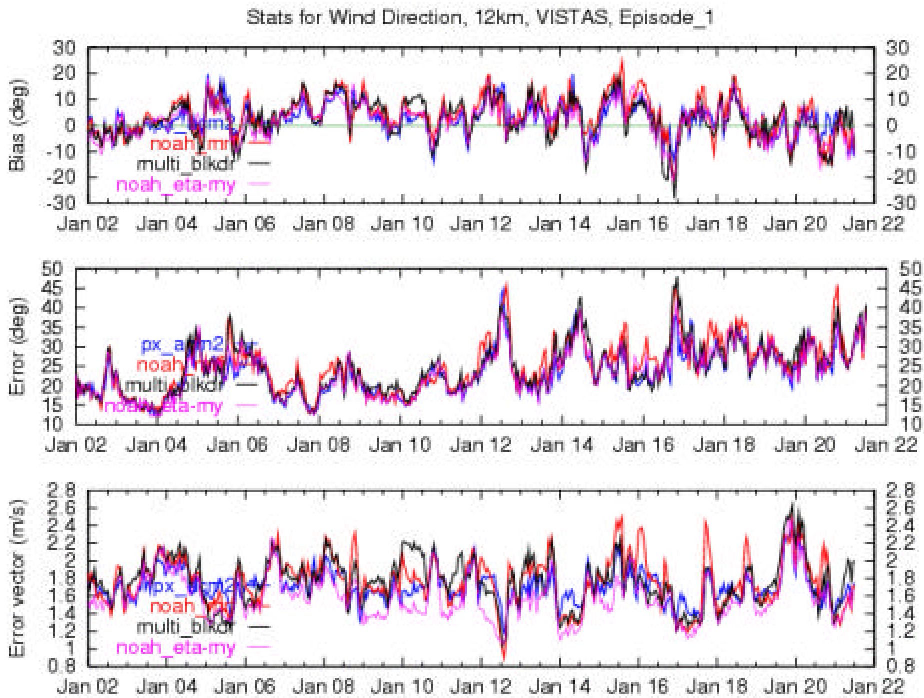

Figure 22. Episode 1 (Jan 2-21, 2002) cross-sensitivity statistical time series plot for winds is shown. The top panel shows wind direction bias, the second panel absolute wind direction error, and the bottom panel the magnitude of the error wind vector. The px_acm2 case is shown in blue, noah_mrf in red, multi_blkdr in black, and noah_eta-my in purple.

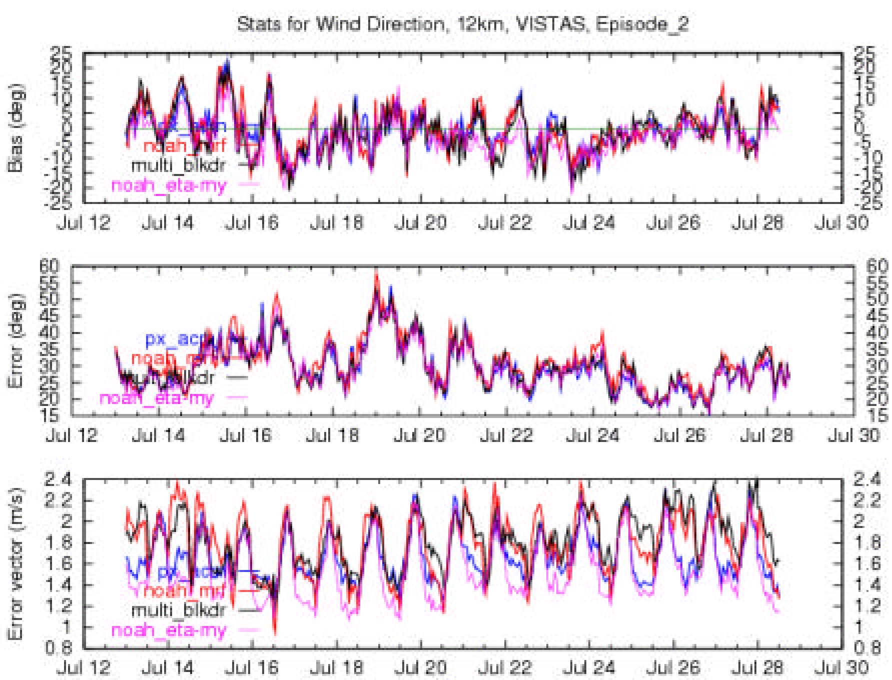

Figure 23. Episode 2 (Jul 13-28, 2001) cross-sensitivity statistical time series plot for winds is shown. The top panel shows wind direction bias, the second panel absolute wind direction error, and the bottom panel the magnitude of the error wind vector. The px_acm case is shown in blue, noah_mrf in red, multi_blkdr in black, and noah_eta-my in purple.

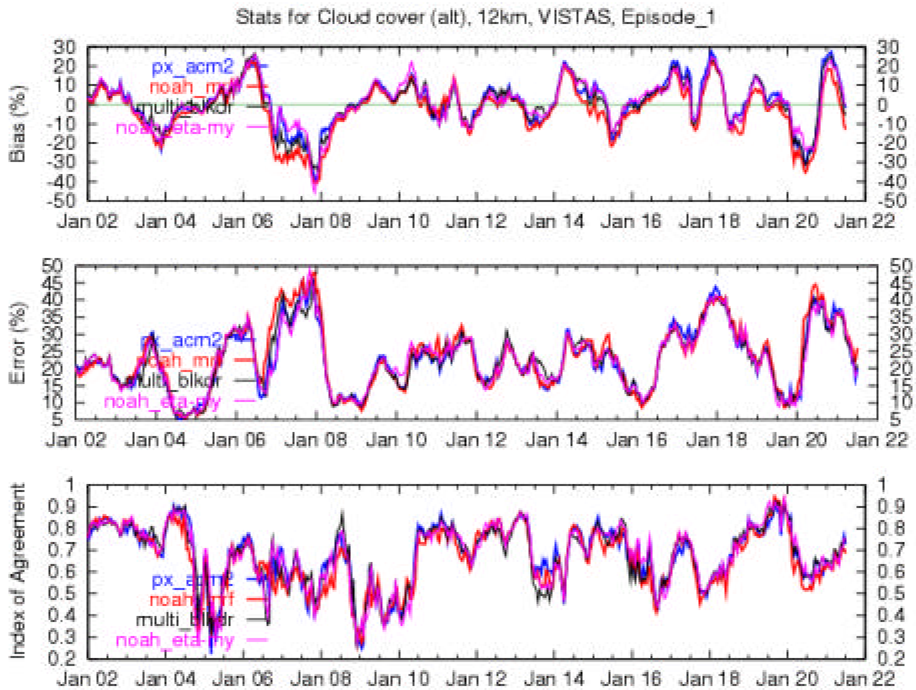

Figure 24. Episode 1 (Jan 2-21, 2002) cross-sensitivity statistical time series plot for cloud coverage is shown. The top panel shows bias, the second panel absolute error, and the bottom panel index of agreement. The px_acm2 case is shown in blue, noah_mrf in red, multi_blkdr in black, and noah_eta-my in purple.

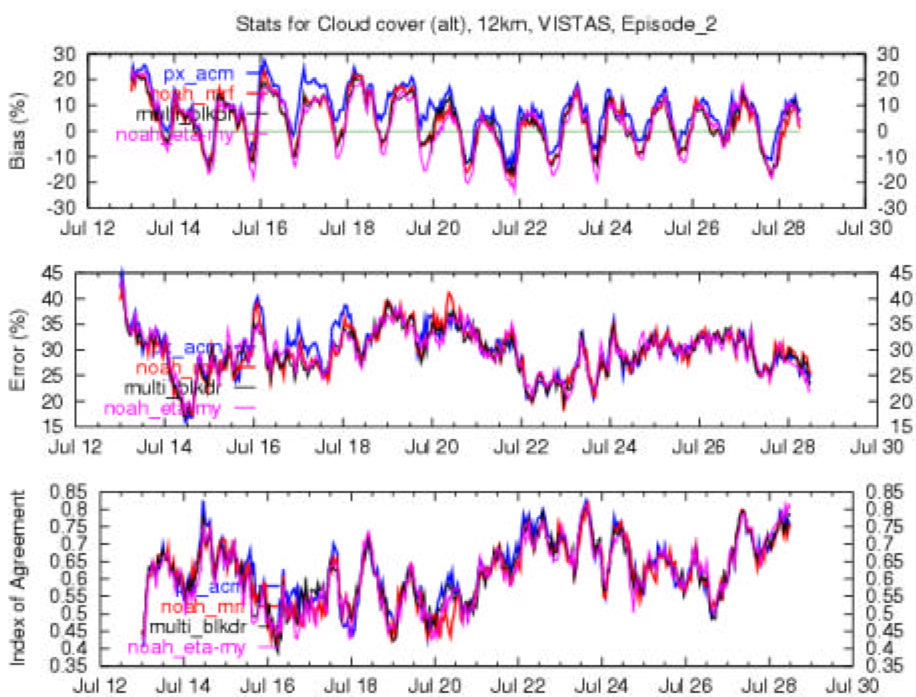

Figure 25. Episode 2 (Jul 13-28, 2001) cross-sensitivity statistical time series plot for cloud coverage is shown. The top panel shows bias, the second panel absolute error, and the bottom panel index of agreement. The px_acm case is shown in blue, noah_mrf in red, multi_blkdr in black, and noah_eta-my in purple.

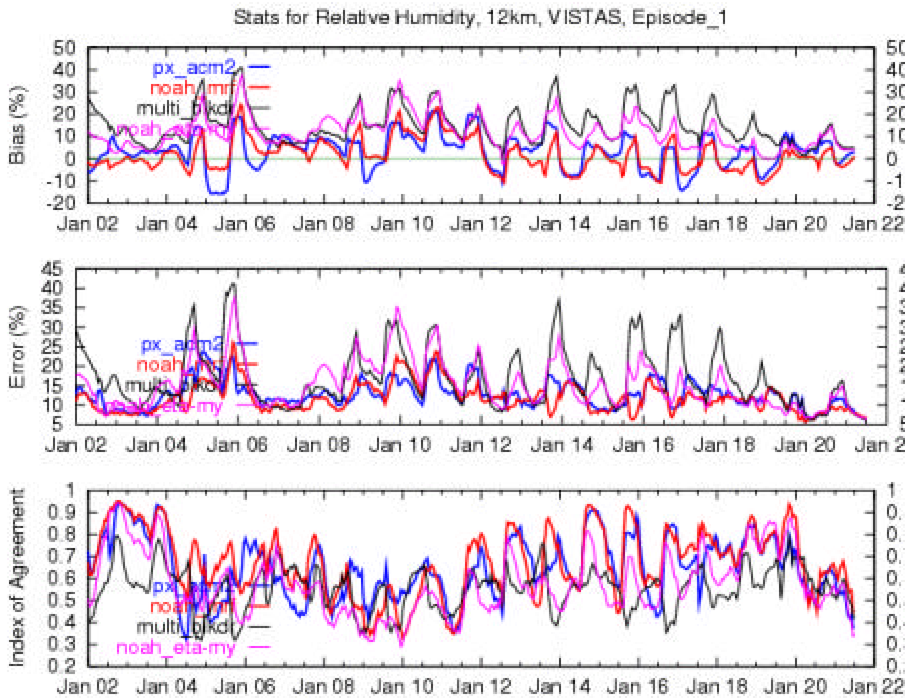

Figure 26. Episode 1 (Jan 2-21, 2002) cross-sensitivity statistical time series plot for relative humidity is shown. The top panel shows bias, the second panel absolute error, and the bottom panel index of agreement. The px_acm2 case is shown in blue, noah_mrf in red, multi_blkdr in black, and noah_eta-my in purple.

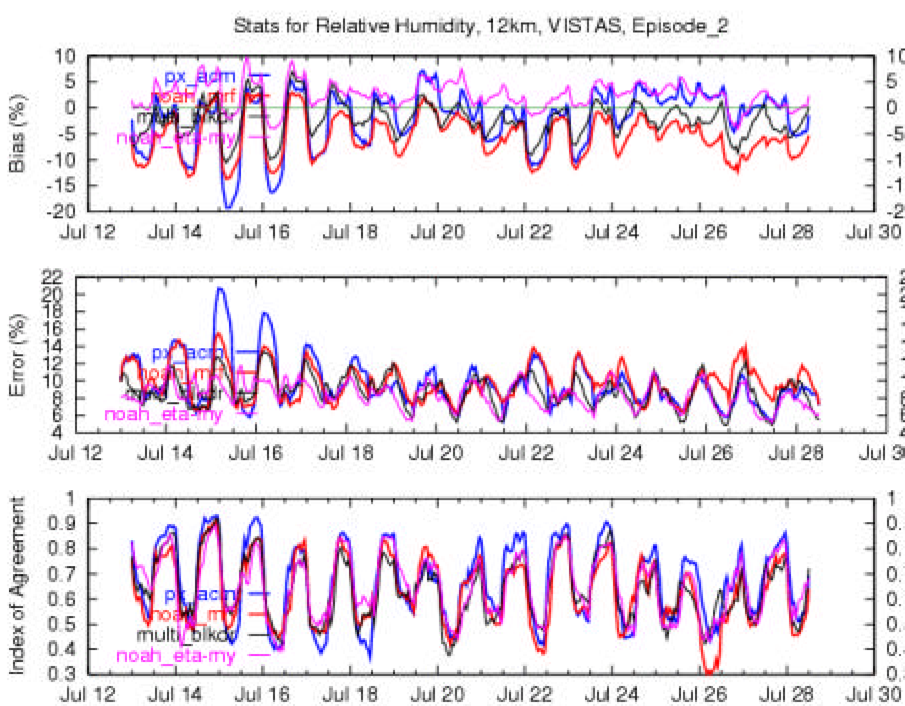

Figure 27. Episode 2 (Jul 13-28, 2001) cross-sensitivity statistical time series plot for relative humidity is shown. The top panel shows bias, the second panel absolute error, and the bottom panel index of agreement. The px_acm case is shown in blue, noah_mrf in red, multi_blkdr in black, and noah_eta-my in purple.

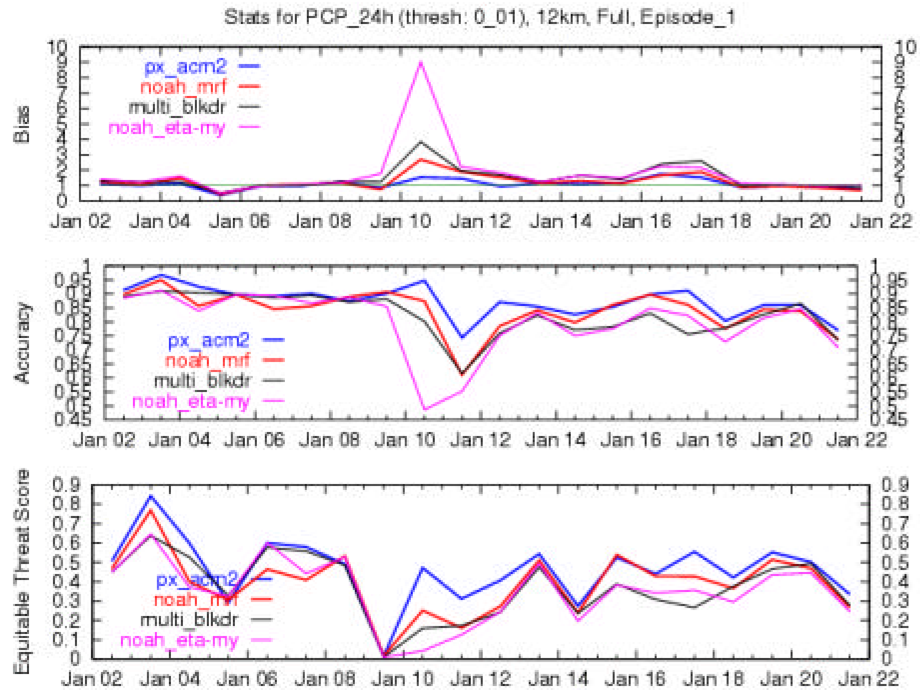

Figure 28. Episode 1 (Jan 2-21, 2002) cross-sensitivity statistical time series plot for 24-h measurable precipitation is shown. The top panel shows bias, the second panel accuracy, and the bottom panel equitable threat score. The px_acm2 case is shown in blue, noah_mrf in red, multi_blkdr in black, and noah_eta-my in purple.

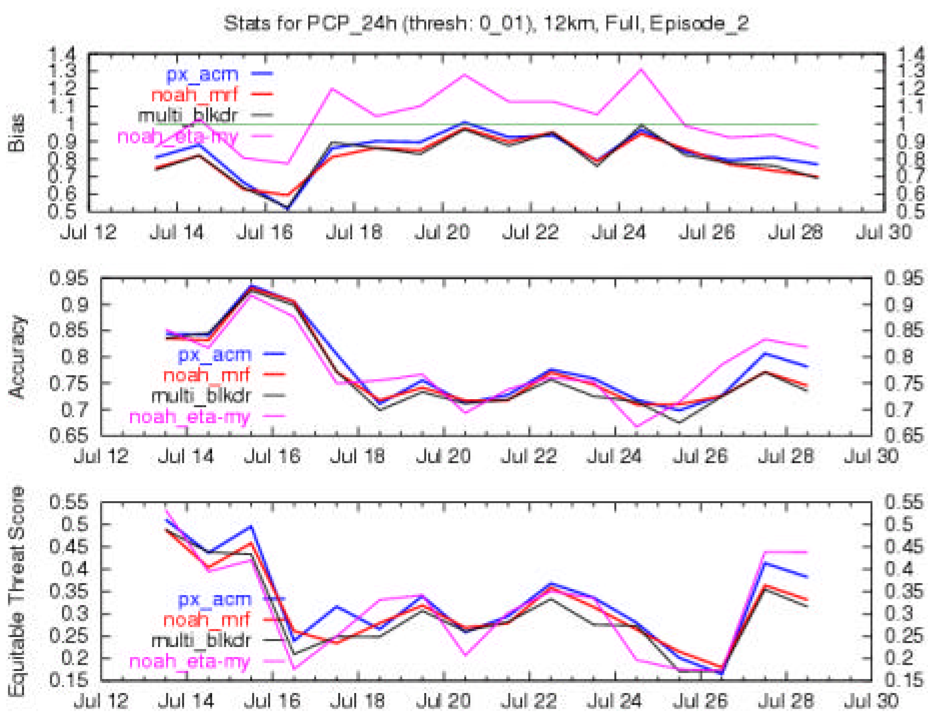

Figure 29. Episode 2 (Jul 13-28, 2001) cross-sensitivity statistical time series plot for 24-h measurable precipitation is shown. The top panel shows bias, the second panel accuracy, and the bottom panel equitable threat score. The px_acm case is shown in blue, noah_mrf in red, multi_blkdr in black, and noah_eta-my in purple.

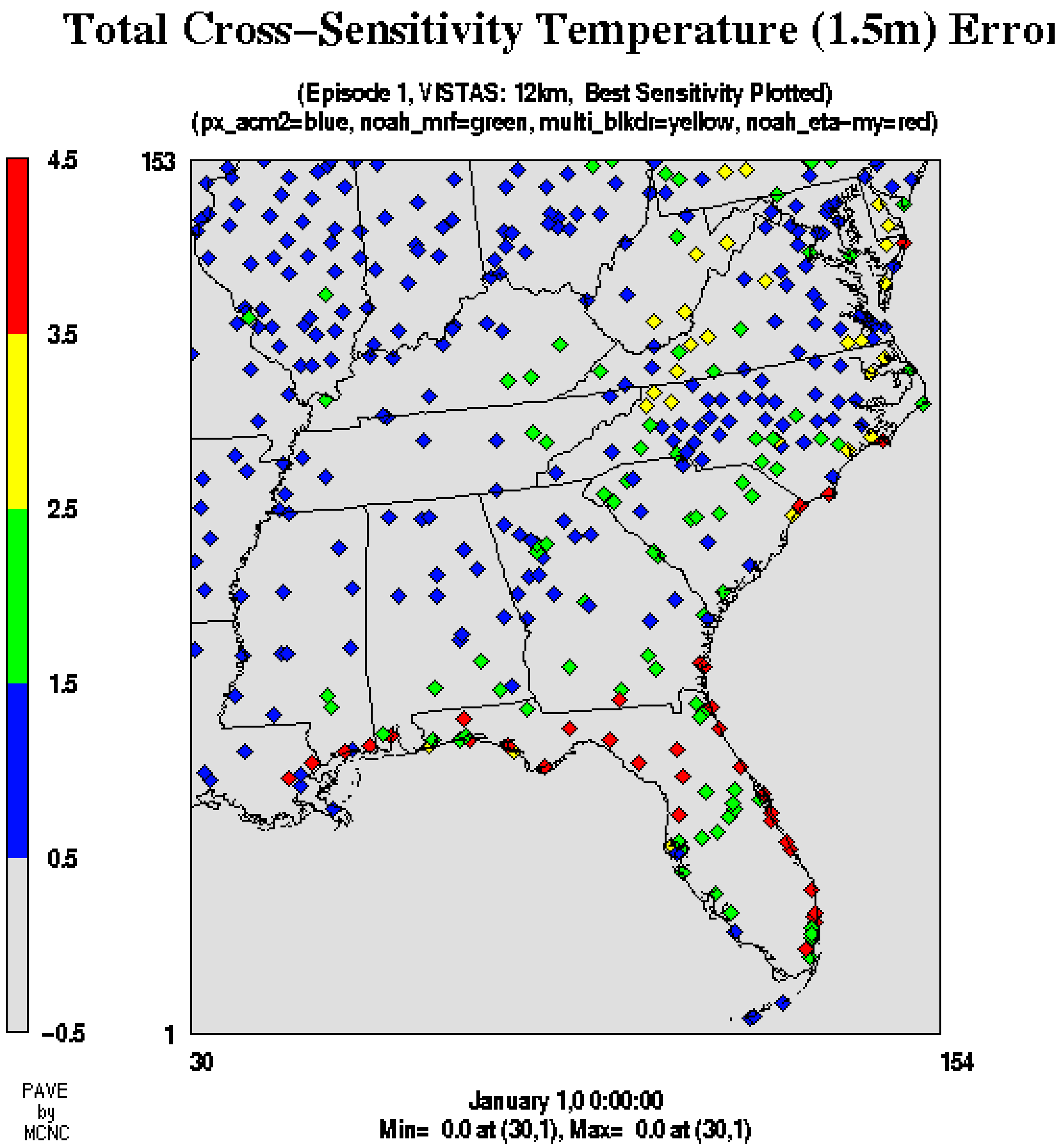

Figure 30. Episode 1 (Jan 2-21, 2002) cross-sensitivity 1.5m temperature absolute error comparison plot is shown. Stations for which px_acm2 show the smallest composite error are plotted in blue, noah_mrf in green, multi_blkdr in yellow, and noah_eta-my in red. The date/time/max/min information at the bottom of the plot serves only as placeholders and should be ignored.

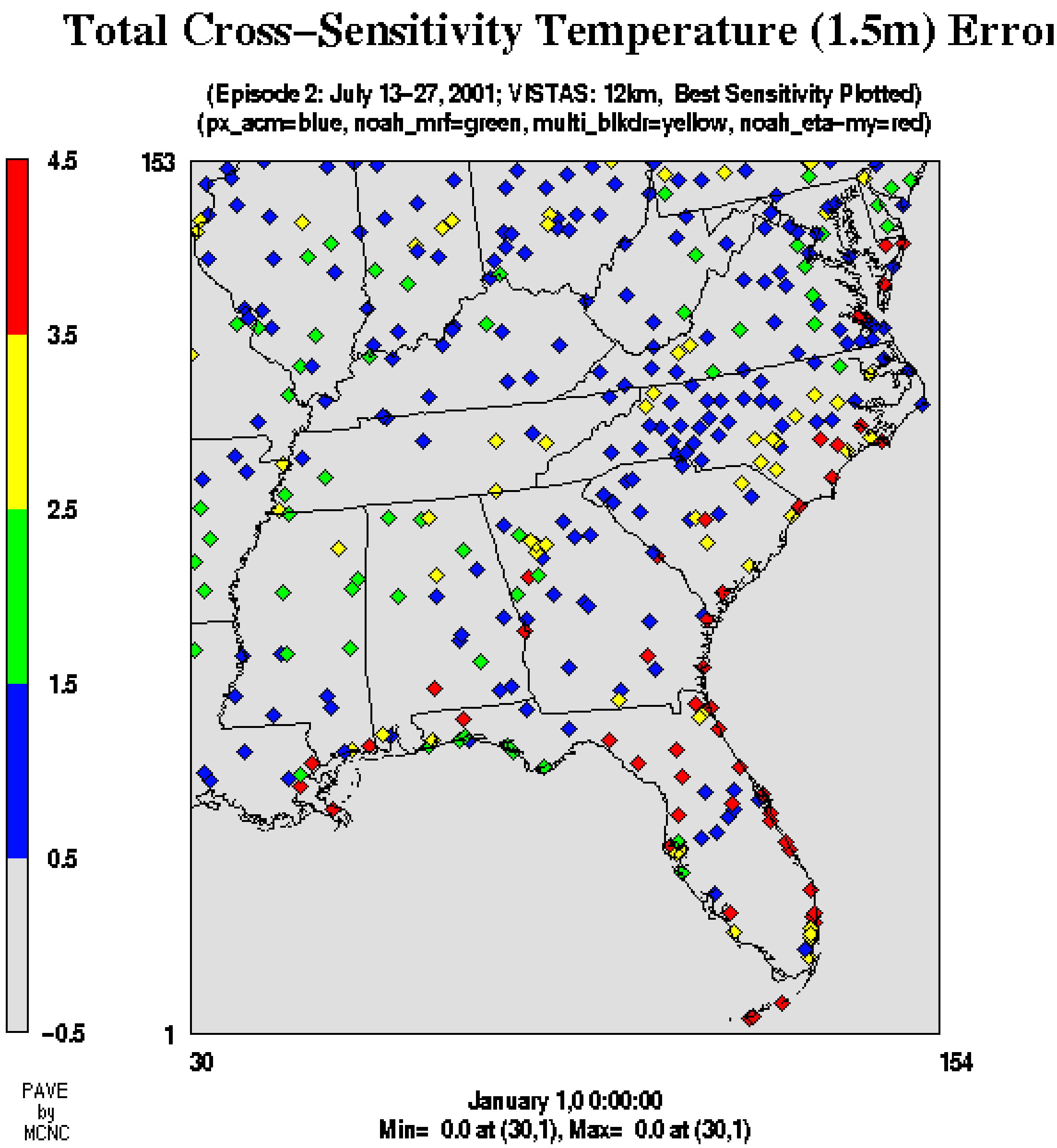

Figure 31. Episode 2 (Jul 13-28, 2002) cross-sensitivity 1.5m temperature absolute error comparison plot is shown. Stations for which px_acm2 show the smallest composite error are plotted in blue, noah_mrf in green, multi_blkdr in yellow, and noah_eta-my in red. The date/time/max/min information at the bottom of the plot serves only as placeholders and should be ignored.

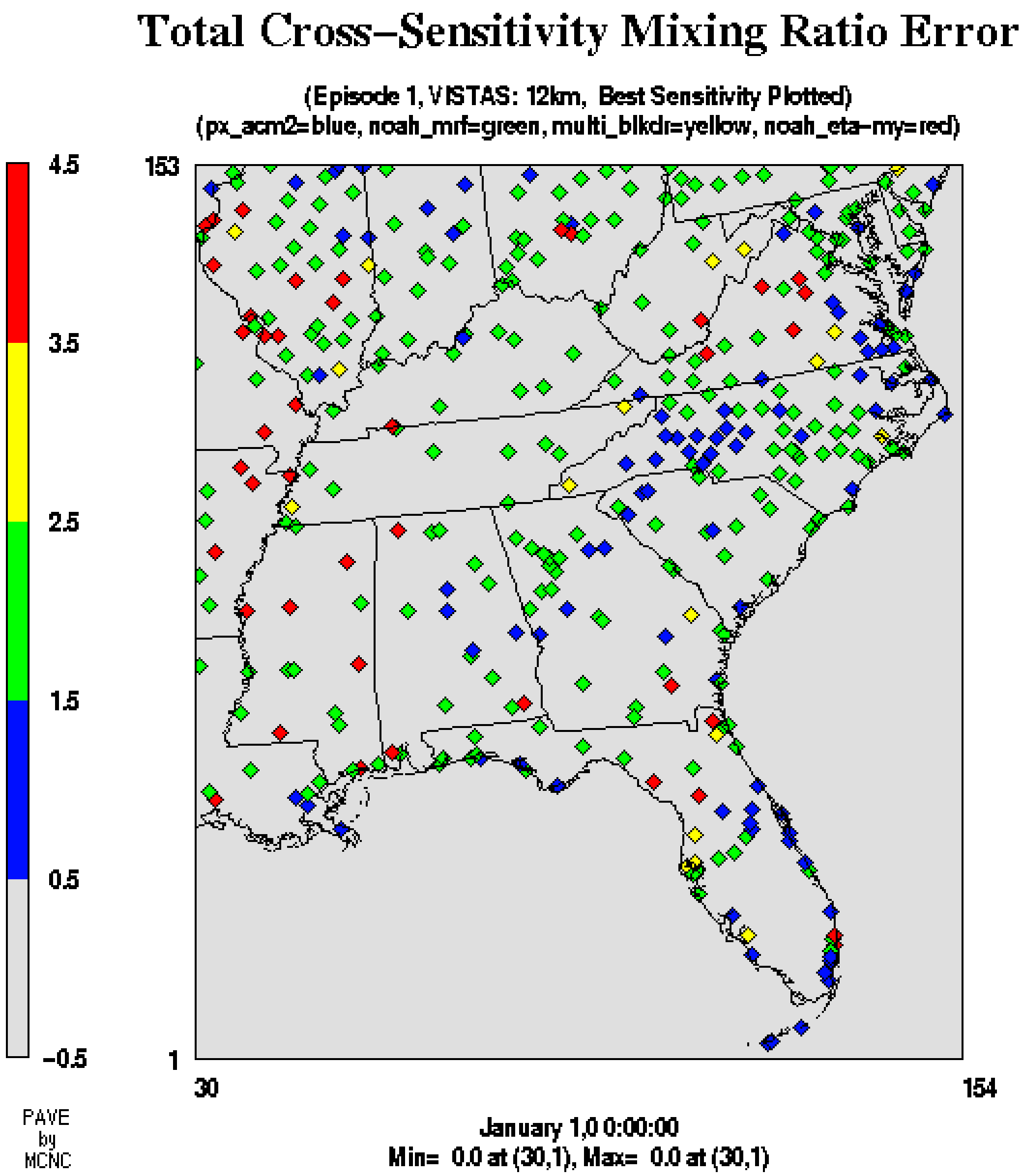

Figure 32. Episode 1 (Jan 2-21, 2002) cross-sensitivity mixing ratio absolute error comparison plot is shown. Stations for which px_acm2 show the smallest composite error are plotted in blue, noah_mrf in green, multi_blkdr in yellow, and noah_eta-my in red. The date/time/max/min information at the bottom of the plot serves only as placeholders and should be ignored.

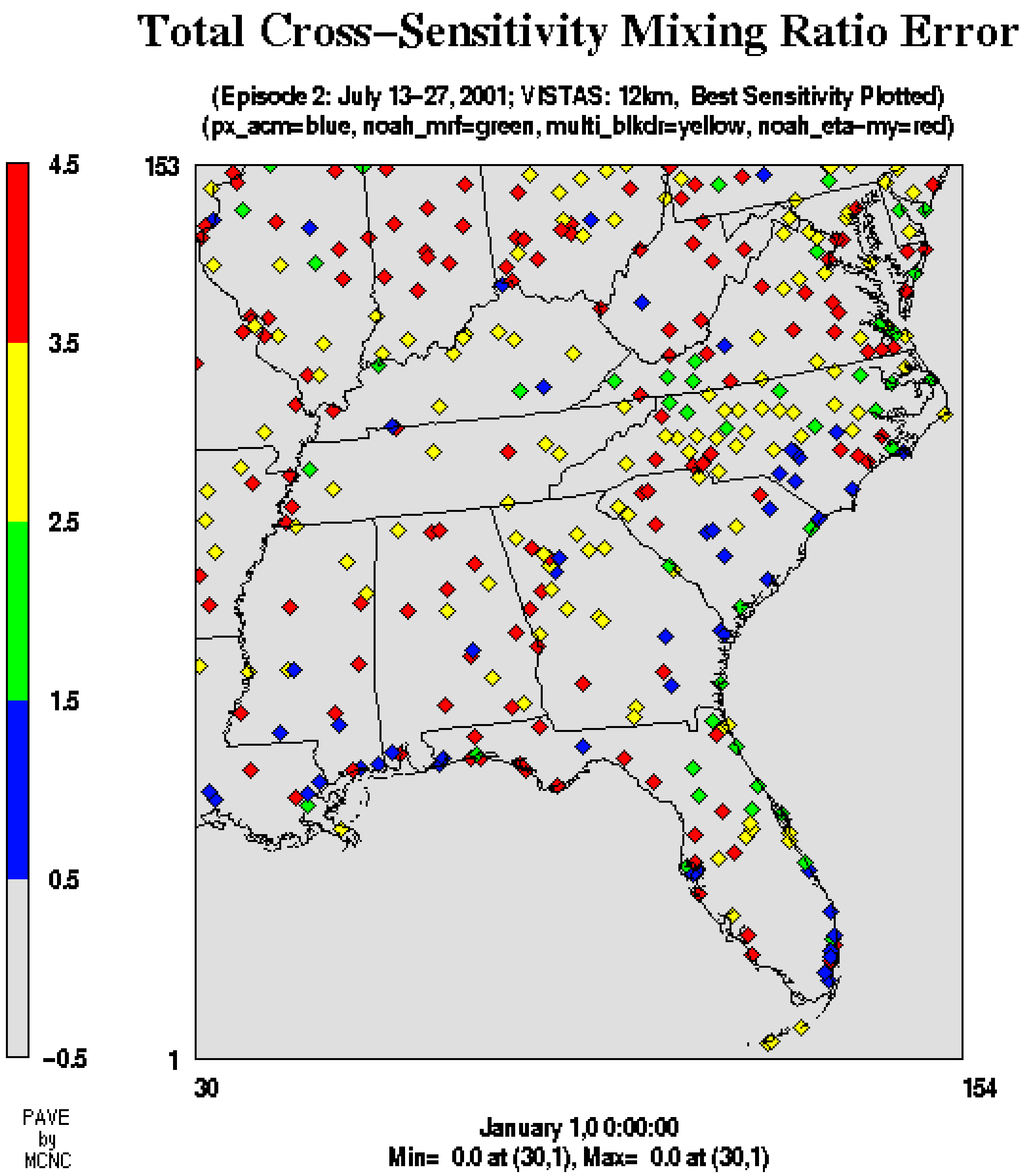

Figure 33. Episode 2 (Jul 13-28, 2001) cross-sensitivity mixing ratio absolute error comparison plot is shown. Stations for which px_acm2 show the smallest composite error are plotted in blue, noah_mrf in green, multi_blkdr in yellow, and noah_eta-my in red. The date/time/max/min information at the bottom of the plot serves only as placeholders and should be ignored.

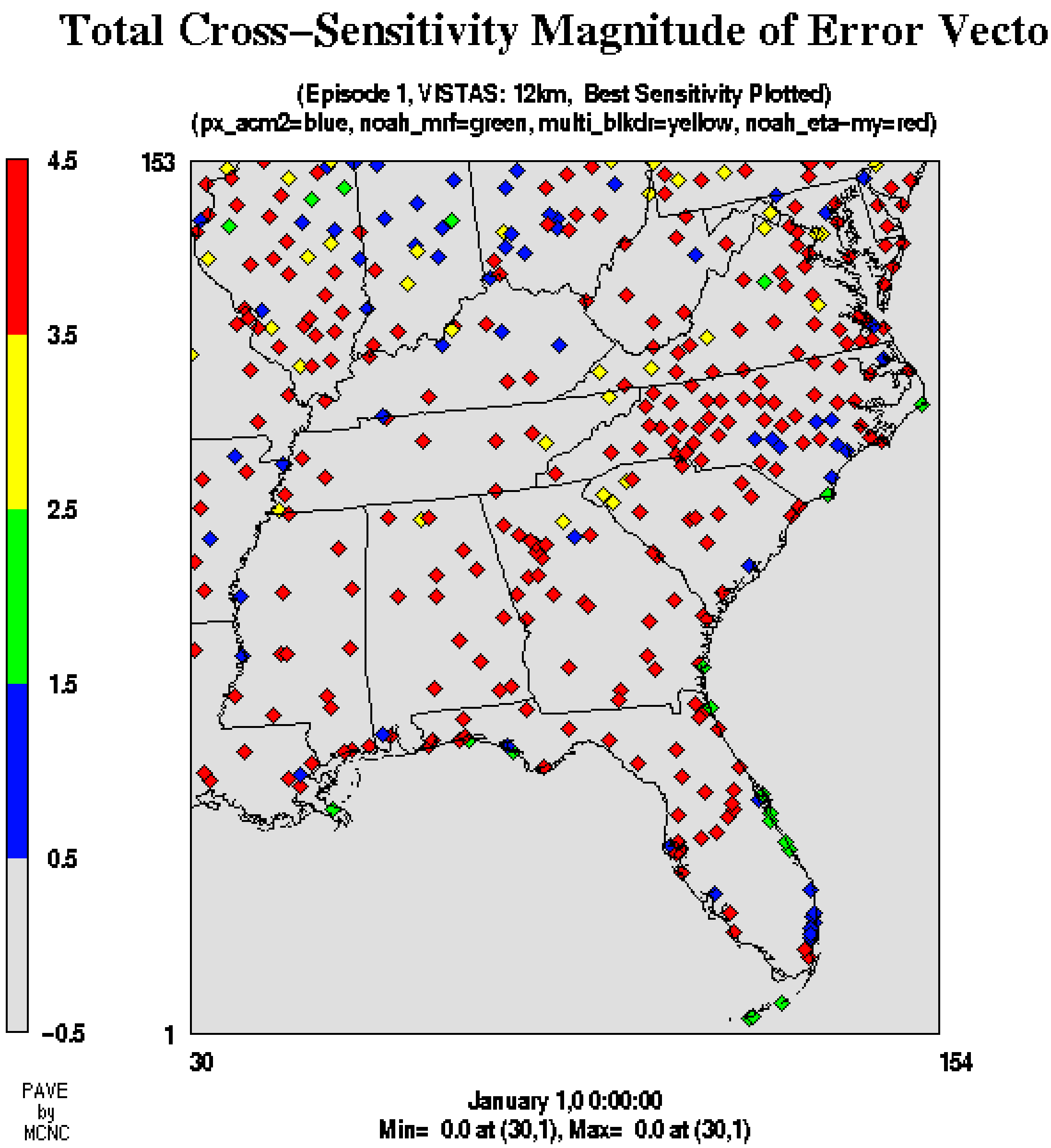

Figure 34. Episode 1 (Jan 2-21, 2002) cross-sensitivity error vector magnitude comparison plot is shown. Stations for which px_acm2 show the smallest composite error are plotted in blue, noah_mrf in green, multi_blkdr in yellow, and noah_eta-my in red. The date/time/max/min information at the bottom of the plot serves only as placeholders and should be ignored.

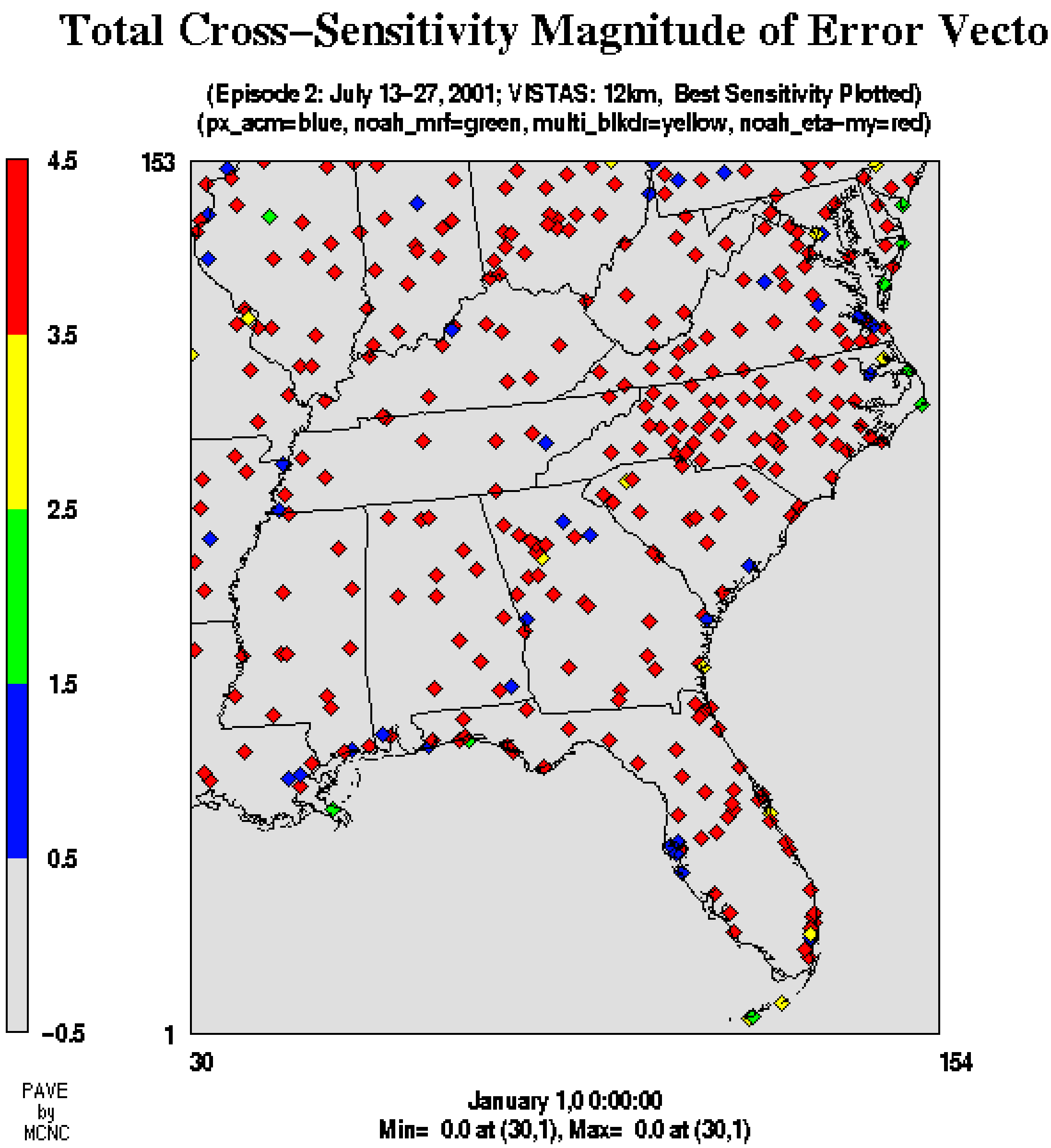

Figure 35. Episode 2 (Jul 13-28, 2001) cross-sensitivity error vector magnitude comparison plot is shown. Stations for which px_acm2 show the smallest composite error are plotted in blue, noah_mrf in green, multi_blkdr in yellow, and noah_eta-my in red. The date/time/max/min information at the bottom of the plot serves only as placeholders and should be ignored.

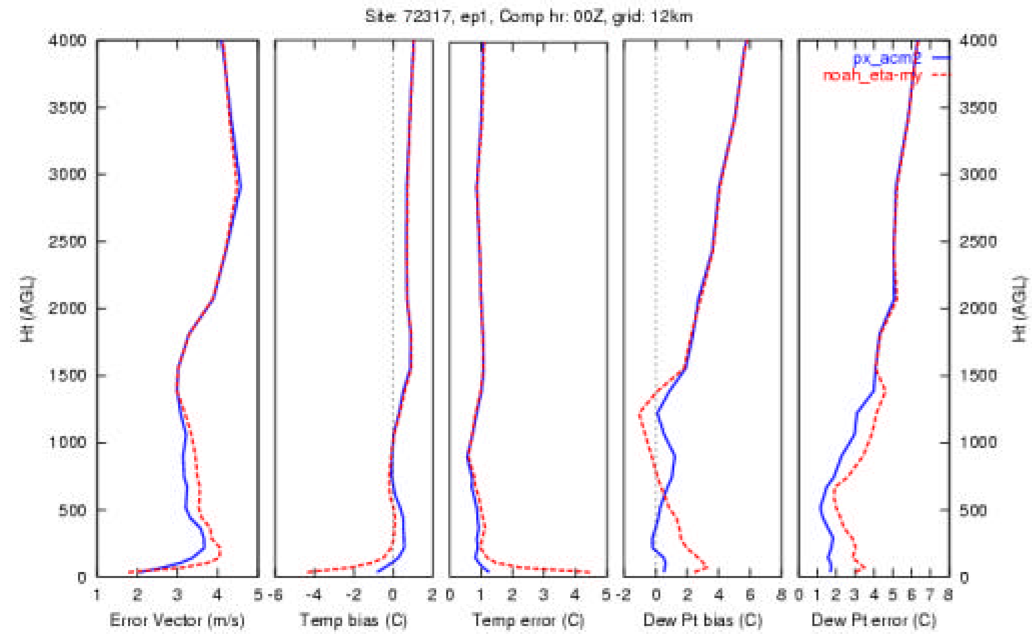

Figure 36. Episode 1 (Jan 2-21, 2002) composite vertical statistics for all 00 UTC times for Greensboro, NC are shown. The magnitude of the error vector is plotted in the leftmost panel, followed by temperature bias and error, then dew point bias and error. Blue represents the px_acm2 case, while dashed red shows the noah_eta-my results.

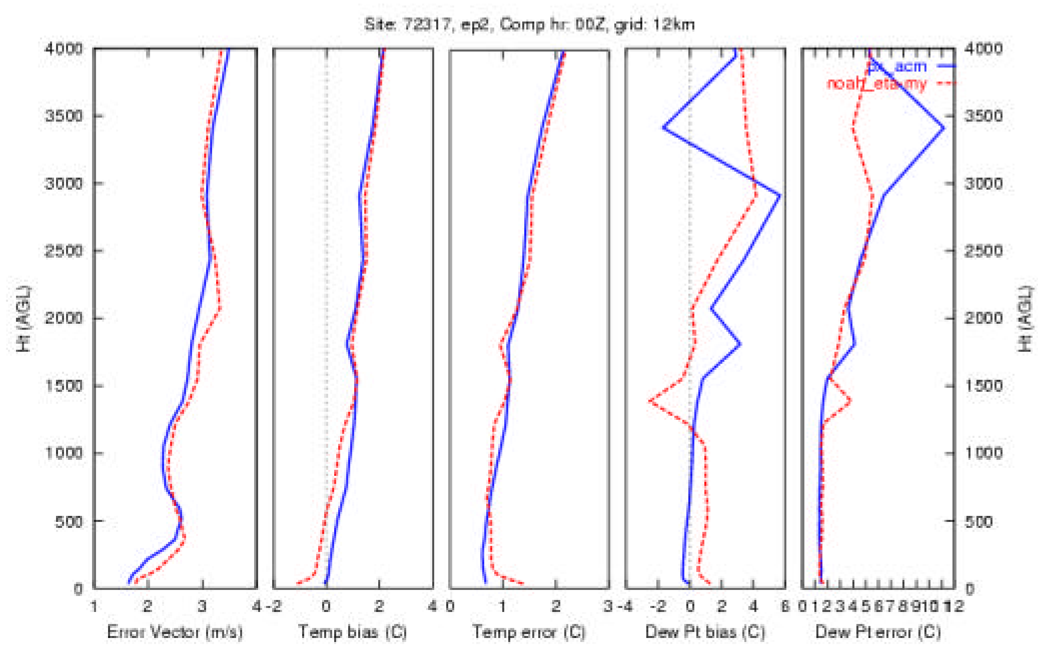

Figure 37. Episode 2 (Jul 13-28, 2001) composite vertical statistics for all 00 UTC times for Greensboro, NC are shown. The magnitude of the error vector is plotted in the leftmost panel, followed by temperature bias and error, then dew point bias and error. Blue represents the px_acm2 case, while dashed red shows the noah_eta-my results.